AD-A251 899

②

# FINAL REPORT
# VISCOELASTIC COMPOSITES
### Dynamic and acoustic properties
### of cellular materials with negative Poisson's ratio

DTIC
ELECTE
S   JUN 1 8 1992
C   D

by

R. S. Lakes, Ph.D., Professor

Department of Mechanical Engineering

Department of Biomedical Engineering

Center for Laser Science and Engineering

University of Iowa

Iowa City, IA 52242

28 July 1991

Submitted to

92 6 11 031

92-15302

# Summary

This report contains the following group of manuscripts which present the work performed during the project period. Also included are the results of a study on polymer negative Poisson's ratio foam conducted by the David Taylor Laboratory, and several earlier viscoelastic studies by the present author.

Lakes, R.S., "Deformation mechanisms of negative Poisson's ratio materials: structural aspects", J. Materials Science, 26: 2287-2292 (1991).

Chen, C.P. and Lakes, R.S., "Holographic study of conventional and negative Poisson's ratio metallic foams: elasticity, yield, and micro-deformation", J. Materials Science, accepted (1990).

Chen, C.P. and Lakes, R.S., "Analysis of high loss viscoelastic composites", submitted

Chen, C.P. and Lakes, R.S., "Viscoelastic behavior of composite materials with conventional or negative Poisson's ratio foam as one phase", submitted

Chen, C.P. and Lakes, R.S., "Holographic study of micro-deformation of metallic negative Poisson's ratio foams" in draft form

The principal conclusions are as follows.

1       Non-affine deformation (in which points in a solid move in a way which cannot be described simply as a strain combined with a rotation) is identified theoretically as a dominant deformation mechanism in materials with negative Poisson's ratios.

2       Non-affine deformation is observed experimentally in materials with negative Poisson's ratios. The effect may be greater or less than that of conventional cellular solids, depending on processing.

3       Non-affine deformation is found theoretically to be essential in achieving high loss combined with high stiffness in composites of a stiff material and a soft, lossy material.

4       Viscoelastic properties of copper foam- viscoelastic elastomer composites exceeded the (lower) Voigt limit. Composite based on re-entrant foam exhibited a higher loss than one based on conventional foam.

5       High loss and relatively stiff materials were studied: solder, indium, gallium, and ferrites. A magnetic ferrite exhibited the highest loss tangent at acoustic frequencies.

6       Composites of copper foam with indium or solder exhibited losses close to the Hashin three phase upper bound with the third phase being a residual amount of pore space.

# Holographic study of non-affine deformation in copper foam with a negative Poisson's ratio -0.8

by

C. P. Chen*, Ph.D., Postdoctoral researcher

and

R. S. Lakes§, Ph.D., Professor


*§Department of Mechanical Engineering

§Department of Biomedical Engineering

§Center for Laser Science and Engineering

University of Iowa

Iowa City, IA 52242


§ Address correspondence to R. Lakes

Draft, revised 28 Jan 1991

revised 27 Feb 1992

# Abstract

Micro-deformation studies of conventional and negative Poisson's ratio copper foams were conducted holographically. Inhomogeneous, non-affine deformation was observed holographically in both foam materials. The negative Poisson's ratio material with a permanent volumetric compression ratio 2.2 exhibited a substantially greater non-affine deformation than the conventional material, in contrast to foam with compression ratio 3.0 examined earlier.

# Introduction

Conventional foams, like other ordinary materials, exhibit a positive Poisson's ratio, that is, they become smaller in cross-section when stretched and larger when compressed. Recently, the invention of negative Poisson's ratio foams was reported[1,2,3]. Foam materials based on metal and several polymers were transformed so that their cellular architecture became re-entrant, i.e. with inwardly protruding cell ribs. Foams with re-entrant structures exhibited negative Poisson's ratios as well as greater resilience than conventional foams.

An experimental study by holographic interferometry was reported of the Young's moduli, Poisson's ratios, yield strengths and characteristic lengths associated with inhomogeneous deformation of the conventional and negative Poisson's ratio metallic foams[4]. The Young's modulus and yield strength of the conventional copper foam were comparable to those predicted by microstructural modelling on the basis of cellular rib bending. The re-entrant copper foam exhibited a negative Poisson's ratio as indicated by the elliptic contour fringes on the specimen surface in the bending tests. Inhomogeneous, non-affine deformation was observed holographically in both foam materials.

The present study applies double-exposure holographic interferometry to examine micro-deformation of re-entrant copper foam with a negative Poisson's ratio of -0.8.

# Material and method

Bending experiments were conducted upon re-entrant copper foam specimens at room temperature. The re-entrant structure was transformed as that a maximum value of negative Poisson's ratio -0.8 at a strain level of 0.1% as determined earlier[5] by shadow moiré. The conventional copper foam used was open cell with density 0.715 g cm$^{-3}$, solid volume fraction 0.08, and average cell size 0.4 mm. It is worth noting that the density of copper foam was not uniformly distributed. The density measured on different portions inside a foam block can vary[5] from 0.08 to 0.1. The copper foam was transformed into re-entrant structure by successive applications of small increments of plastic deformation in three orthogonal directions, as described earlier[1,2,3]. The density of the re-entrant copper foam tested here was 1.57 g cm$^{-3}$ with a permanent volumetric compression ratio of approximately 2.2, and solid volume fraction 0.22. The dimensions of the re-entrant copper foam specimen was 5.7mm by 10.8mm in cross section and 35.5mm in length. For the purpose of comparison, a re-entrant foam specimen was annealed at 500°C before being tested. The anneal process did not result in measurable change in the foam dimensions. The dimensions of the annealed re-entrant copper foam specimen was 7.75 mm by 7.9 mm in cross section and 36 mm in length. The specimens were machine finished to obtain the desired surface smoothness.

The experimental study of the re-entrant copper foams by holographic interferometry is as described earlier[4]. The specimen was deformed by a nearly pure bending moment. The zero-order fringe method [ZF][6] was used to obtain the specimen's Young's moduli and Poisson's ratios from the fringe pattern on the strained surface of the specimen. The non-affine deformation of the re-entrant foam was also studied by the

zero-order fringe method. The inhomogeneous deformation of the non-affine type was visualized as an increase in the bumpiness of the fringes in response to the increasing loads. The results were compared with those obtained earlier[4].

## Results and Discussion

The results of the Young's moduli and Poisson's ratios are listed in Table 1, in comparison with the previous results for the re-entrant copper foam with a permanent volumetric compression ratio of approximately three[4]. Each Young's modulus was determined at two strain levels. The Young's modulus remained approximately constant when the strain level was increased. For the non-annealed re-entrant copper foam, the Young's modulus was found to be 390 MPa at a macroscopic strain of $1.4 \times 10^{-4}$ and $1.7 \times 10^{-4}$ and 200 MPa at a macroscopic strain of $1.6 \times 10^{-4}$ and $3.0 \times 10^{-4}$, on the strained surface of width 10.8mm and 5.7mm, respectively. For the annealed re-entrant copper foam, the Young's modulus was obtained to be 510 MPa at a macroscopic strain of $9.5 \times 10^{-5}$ and $1.8 \times 10^{-4}$; and 245 MPa at a macroscopic strain $9.7 \times 10^{-5}$ and $1.8 \times 10^{-4}$, on the strained surface of width 7.9mm and 7.75mm, respectively. In the previous results[4] for the re-entrant copper foam with a permanent volumetric compression ratio of approximately 3, the Young's modulus was obtained to be 480 MPa at a macroscopic strain of $6.7 \times 10^{-4}$.

The Young's moduli obtained from bending in two orthogonal directions differed by a factor of two. Anisotropy will not give rise to such an effect since a bending experiment in any transverse direction discloses the Young's modulus for strain along the beam axis even if the beam is anisotropic. Anisotropy could arise from different permanent compression in the three orthogonal directions, however care was taken to avoid that. Nonuniformity in the permanent compression process could give rise to such results.

The fringe pattern obtained for these current tests were observed to be bumpier than that obtained previously[4]. The comparison of the clarity of the fringes of the re-entrant foams was shown in Figure 1. The non-affine motion disclosed by these experiments is an average value perpendicular to the specimen surface. The maximum strain level for the minimum observable clarity of the fringe pattern was $2.5 \times 10^{-4}$, well below $9.2 \times 10^{-4}$ as obtained previously[4] for re-entrant foam of a higher permanent volumetric compression. The Poisson's ratio for both non-annealed and annealed re-entrant copper foams could not be determined in this experiment since the fringes could only be recognized at a low macroscopic strain level. At low strain, only a small part of the elliptic fringes was visible on the surface and therefore the Poisson's ratio were not obtainable. However, the Poisson's ratio of this type of re-entrant copper foam was determined to be -0.8 by the shadow moire test earlier[5].

Quantitative measures of such inhomogeneous deformation may be defined as follows: the ratio $\Gamma$ of micro-strain to macro-strain $\varepsilon_{macro}$, $\Gamma = (\delta/d_{cell})/\varepsilon_{macro}$; and a micro-deformation characteristic length $\ell_m = \delta/\varepsilon_{macro}$ in which $\delta$ is the inhomogeneous micro-deformation and $d_{cell}$ is the cell size. In the present zero-order fringe experiments the fringes become totally fragmented when the micro-deformation over one cell is one fringe or half a wavelength of red light, so $\delta = 0.3$ μm. The cell size is 0.4 mm for conventional foam and $0.4mm/(2.2)^{1/3}$ for the present re-entrant foam. Consequently, for the conventional copper foam[4], $\Gamma_{avg,\perp} = 2.1$, and $\ell_m = 0.86$mm; for the previous re-entrant foam of permanent compression ratio 3, $\Gamma_{avg,\perp} = 1.3$, $\ell_m = 0.38$mm; for the present re-entrant foam, $\Gamma_{avg,\perp} = 3.9$, $\ell_m = 4$ mm. So in the present

re-entrant foam, both measures of the degree of inhomogeneous deformation are greater than in the case of conventional foam or a previous re-entrant foam.

The inhomogeneous, non-affine micro-deformation observed in the foams has several interesting implications as discussed in more detail in an earlier communication[4]. Micro deformation is evidence of generalized continuum behavior in the material[7]. The micro-deformation and local rotation degrees of freedom of these materials are intimately connected with a toughening mechanism governed by redistribution of stress around cracks and holes.

## CONCLUSIONS

1. Negative Poisson's ratio copper foam with a permanent volumetric compression ratio of 2.2 exhibits a greater non-affine deformation than either conventional foam or negative Poisson's ratio foam with a volumetric compression ratio of 3.

## ACKNOWLEDGMENT

## References

1. R.S. Lakes, *Science* **235** (1987) 1038.
2. R.S. Lakes, *Science* **238** (1987) 551.
3. E.A. Friis, R.S. Lakes and J.B. Park, *J. Materials Science* **23** (1988) 4406.
4. C.P. Chen and R.S. Lakes, "Holographic study of conventional and negative Poisson's ratio metallic foams: elasticity, yield, and micro-deformation", *J. Materials Science*, **26** (1991) 5397-5402
5. J. B. Choi and R. S. Lakes, "Nonlinear properties of polymer cellular materials with a negative Poisson's ratio", *J. Materials Science*, accepted (1991).
6. W. Schumann and M.Dubas, "Holographic interferometry" (Springer-Verlag, 1979), Berlin.
7. R. D. Mindlin, "Microstructure in linear elasticity", *Arch. Rational Mech. Anal.* **16**, (1964) 51-78

# Table 1. Specimen dimensions and properties

Width of strained surface is last dimension in 'specimen size'.

| Specimen | Specimen size ( mm ) | Permanent Compression ratio | Poisson's ratio | Young's modulus $E$ | Inhomogeneous deformation $\Gamma$ |
|---|---|---|---|---|---|
| Re-entrant copper foam | 26 x 6 x 6.5 | 3.0 | -0.11 | 480 MPa | 1.3 |
| Re-entrant copper foam | 35.5 x 5.7 x 10.8 | 2.2 | N/A | 390 MPa | |
| | 35.5 x 10.8 x 5.7 | | | 200 MPa | |
| Re-entrant copper foam annealed at 500°C | 36 x 7.75 x 7.9 | 2.2 | N/A | 510 MPa | 3.9 |
| | 36 x 7.9 x 7.75 | | | 245 MPa | |
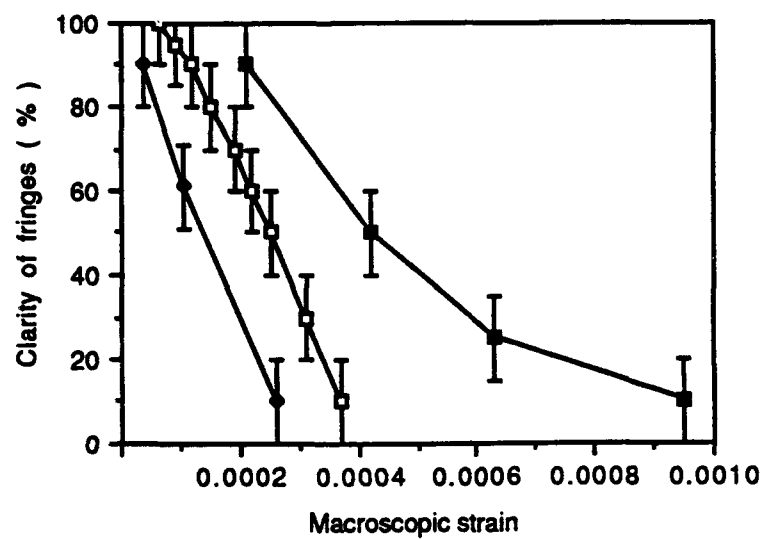
# Viscoelastic behavior of composite materials with conventional or negative Poisson's ratio foam as one phase

by

C. P. Chen*, Ph.D., Postdoctoral researcher

and

R. S. Lakes§, Ph.D., Professor


*§Department of Mechanical Engineering

§Department of Biomedical Engineering

§Center for Laser Science and Engineering

University of Iowa

Iowa City, IA 52242


§ Address correspondence to R. Lakes

29 July 1991

revised 2 May 1992

## Synopsis

This article describes experimental investigations of viscoelastic properties of composites consisting of conventional and re-entrant negative Poisson's ratio copper foam as a matrix, with high loss filler materials: viscoelastic elastomer, solder, and indium. Viscoelastic properties of gallium and several ferrites were determined as well. The loss tangent of the copper- elastomer composite substantially exceeded the (lower) Voigt limit; the loss tangent of the copper-solder and copper-indium composites were close to the (upper) Hashin limit for two solid phases and one pore phase.

# INTRODUCTION

In an accompanying article we have considered predictions of viscoelastic behavior of composite materials with various structures (Chen and Lakes,1992). Structures which give rise to the highest viscoelastic loss tangent have the common feature that the microscopic distribution of strain is nonuniform so that the deformation kinematics of points in the composite is non-affine. The reason that high loss can arise in composites of this type is that the strain in the lossy, compliant phase is higher than the macroscopic strain in the composite. Non-affine deformation is also characteristic of the recently developed foam materials with negative Poisson's ratios (Lakes, 1987, 1991). Experimental studies of the conventional and negative Poisson's ratio copper foams by holographic interferometry showed that inhomogeneous, non-affine deformation occurred in the ribs of copper foams (Chen and Lakes, in press).

The present work is directed at the exploration of model composite materials which exhibit non-affine deformation with the ultimate aim of development of composites with high stiffness and high loss. To that end, we investigate the dynamic viscoelastic properties of composites of both conventional and negative Poisson's ratio copper foams filled with materials of known high loss. This is in contrast to all earlier studies on such foams, which have considered the foam skeleton only, without a second solid phase.

# MICROMECHANICS APPARATUS METHOD

The experimental method made use of a micromechanics apparatus originally developed for the study of Cosserat elasticity in composites, and evolved for the study of viscoelastic materials (Chen and Lakes,1991). The apparatus and associated analysis scheme is capable of determining the viscoelastic properties of a material isothermally, with a single apparatus, over 10 decades of time and frequency. Torque was applied to the specimen electromagnetically and its deformation was determined by laser

interferometry. Resonances were eliminated from the torque and angle measuring devices by this approach. Resonances remaining in the specimen itself were corrected by a numerical analysis scheme based on an analytical solution which is applicable to homogeneous cylindrical specimens of any degree of loss. The apparatus is capable of creep, constant load rate, subresonant dynamic, and resonant dynamic experiments in bending and torsion. The range of equivalent frequency for torsion is from less than $10^{-6}$ Hz to about $10^4$ Hz.

Analysis of the data to obtain the material's complex shear modulus $G^* = |G^*|(1 + i \tan \delta)$ is based on a numerical inversion of the following exact relation for the torsional dynamics of a viscoelastic cylinder (Christensen, 1982).

$$\frac{M^*}{\Phi} = I_{sp} \omega^2 h \frac{\cot \Omega^*}{\Omega^*} - I_{at} \omega^2 \qquad (1)$$

in which $M^*$ is the measured sinusoidal torque applied, $\Phi$ is the measured end angular displacement, $I_{sp}$ is the mass moment of inertia of the specimen, $\omega$ is the angular frequency in radians per second, $\Omega^* = [\rho \omega^2 h^2 / KG^*]^{1/2}$, $\rho$ is the mass density of the specimen, h is the length of the specimen, K is a geometrical constant, 1 for a specimen with circular cross section; 0.8 for a specimen with square cross section, $G^*$ is the complex shear modulus, and $I_{at}$ is the mass moment of inertia of the end attachment. This analysis scheme incorporates the assumption of a continuous viscoelastic medium. The foams are not continuous, but a difference would not become apparent until the resonant frequency of the foam ribs is approached, at frequencies well above those used here. The phase angle between stress and strain was measured with an oscilloscope, as in earlier studies. The resolution of the phase angle on the oscilloscope was approximately 0.7°, or a corresponding $\tan \delta$ of 0.012. The loss tangent of low loss specimens was therefore not obtainable by this method under subresonant conditions at low frequencies. A digital lock in amplifier was tried to improve phase resolution, but it generated unacceptable phase errors. A different brand of lock in amplifier is now being evaluated. The phase resolution was considered adequate for the purposes of this study.

Data reduction in the case of small loss (i.e., $\tan \delta \ll 1$) becomes considerably simplified (Christensen, 1982) and errors due to phase uncertainty are reduced (Chen and Lakes, 1991) in the vicinity of resonance

$$\sqrt{3} \tan \delta \approx \frac{\Delta \omega}{\omega_0} \qquad (2)$$

The loss tangent $\tan \delta$ of low loss materials can therefore be obtained from a specimen of proper size with an external inertia at a resonant frequency via Equation (2). In this

4

study, frequencies associated with vibration and acoustic signals are of particular interest, therefore the lengthy creep experiments used in previous studies are omitted. Experiments were conducted at room temperature (22°C ± 2°C); for each individual test the temperature was constant to within 0.5°C.

# MATERIALS

Materials studied included conventional and re-entrant copper foam, solid brass, a high-loss viscoelastic elastomeric polymer, solder (PbSn, 60:40), indium, gallium, and several ferrites. The rationale for the choice of the metals is that since their melting points are low, viscoelastic loss due to grain boundary motion or stress induced diffusion is to be expected at room temperature.

The foams were cut with a low speed diamond saw (Isomet, inc) into prisms of nearly square cross section. The elastomer was cast in a long rod. The (solid) solder wire was studied in as-received condition. The indium wire was studied in as-received condition; following heating at 240°C and cooling to 20°C; and following melting at 300°C and solidification at -20°C. The gallium was melted and cast into a plastic tubule. The ferrites were cut with a low speed diamond saw into slender prisms of nearly square cross section. The conventional copper foam is open cell with average cell size 1 mm, and density 0.68 g/cm$^3$ or solid volume fraction 7.6%. The re-entrant copper foam with cell size 0.67 mm resulted from a permanent volumetric compression ratio of 1.48. A negative Poisson's as small as -0.8 can be obtained (Choi and Lakes, in press) under these conditions. Specimen sizes were chosen to achieve appropriate structural stiffness for the tests and are shown in Table 1.

Composite specimens were prepared with copper foam as a matrix and polymer, solder, or indium as fillers. In initial trials, the filler metal was heated by a propane torch or in a furnace, with soldering flux, with the aim of incorporating the melted metal in the voids in the foam. This procedure did not fill the entire void space in the foam: composite prepared this way had over 50% void volume. Composite foams with low void content were prepared by heating the copper foams and the filler metals in an evacuated glass tube in an oven. This procedure prevented surface oxidation of the copper and improved wetting. The filler metals were melted at approximately 200°C and deposited into the copper foams by gravity. No oxidation was observed. The void content in the composite foams thus made was found to be less than 15% by volume. Voids with diameter from 0.025 mm to 0.1 mm were observed microscopically to be scattered inside the foams. No discontinuities between the copper matrix and filler were

observed. The injection of viscoelastic elastomer into the copper foams was made courtesy of Polymer Dynamics, Inc, Lehigh Valley, PA.

## RESULTS AND DISCUSSION

The dynamic shear modulus $|G^*|$ of solid copper at 1 kHz was found to be 40 GPa and the loss tangent tanδ was 0.002. The loss tangent tanδ of copper at 0.1 Hz is given as about 0.0001 (Smithells, 1976).

Dynamic shear moduli $|G^*|$ and loss tangent tanδ vs frequency of foams and solid filler materials derived from torsional tests are shown in Figures 1-8. The maximum errors in $|G^*|$ and tanδ due to the uncertainties in the specimen geometry and measurement accuracies are shown as error bars in Figures 1-9 and 13. Where no error bar is shown, the estimated error is smaller than the thickness of the data points. Specimen resonances are denoted by downward pointing arrows. Figure 1 shows results for copper foams of conventional and re-entrant structures. It is observed that the copper foams behave somewhat differently from solid copper: $|G^*|$ and tanδ increased substantially at high frequencies. Conventional copper foam exhibits higher $|G^*|$ than the re-entrant copper foam, which is similar to results observed for the copper and polymeric foams in the earlier studies (Lakes, 1987). Higher tanδ is obtained at high frequencies for the re-entrant foam than the conventional foam.

Table 2 summarizes stiffness and loss results at selected frequencies for the homogeneous materials studied here as well as the copper foams without any filler. The value of the loss tangent for solid copper at low frequency is from Smithells(1976). Table 3 gives corresponding results for composites based on the foams combined with other materials within the interstices.

Figure 2 shows results for a viscoelastic elastomeric polymer, which exhibits monotonically increasing modulus and loss tangent. The results of the composites of polymer filler and conventional, and re-entrant copper foams are shown in Figure 3. The composites show a loss tangent value between those of the solid polymer and foams. However, it is worth noting that the moduli of the composites are almost twice as large than those of the polymer and the foams. This suggests an effect of non-affine deformation.

Figure 4 shows results for solder. In contrast to the polymeric materials and the copper foams, tanδ of solder decreases when the frequency increases. Figure 5 shows results for the conventional, and re-entrant copper foams combined with large void content solder filler. The moduli of the composites are only slightly higher than those of the foams; these are much lower than the modulus of the solder, 9.72 GPa at 0.1 Hz.

This is as expected since the volumetric fractions of the solder deposited in the foams are low, 22% and 34% for the conventional and re-entrant foams, respectively. Figure 6 shows results for the conventional, and re-entrant copper foams combined with low void content solder filler. The moduli at 0.1 Hz of the composites are 9.3 GPa and 11.9 GPa for composites with the conventional and re-entrant foam matrixes, respectively. The modulus of the composite with the re-entrant copper foam matrix is higher than that with the conventional foam matrix even though the solder fraction in the former is slightly lower than the latter. This is contrast to what observed for the pure copper foams and the composites combined with the much softer polymer.

Figure 7 shows results for indium wire. Figure 8 shows results for the conventional, and re-entrant copper foams combined with large void content indium filler. Increasing the volume fraction of indium results in a much higher modulus and loss tangent for the conventional copper foam composite in comparison with the re-entrant copper foam composite. Figure 9 shows results for the conventional, and re-entrant copper foams combined with low void content indium filler, respectively. The modulus of the re-entrant copper- indium composite is higher than that of the original copper foam; this behavior was similar to that of the copper-solder composite.

Figures 10 and 11 show stiffness-loss maps for the copper foams, filler materials and low void content composites at 0.1 Hz, and 1 kHz, respectively. For the purpose of comparison, a summary of the constituent volume fractions, and the moduli and loss tangents at selected frequencies is listed in Table 3. The moduli of copper foams and polymer composites for the conventional structure were higher than the re-entrant structure. However, the moduli of the solder and indium composites for the conventional structure were higher than the re-entrant structure. The loss tangents tan$\delta$ at 1 kHz were always higher for the re-entrant copper foam composites than the conventional copper foam composites. An exception is the large void content indium filled composites in which the volumetric fraction of the indium deposited in the re-entrant copper foam was only half as that in the conventional copper foam. For the solder and indium filled composites, large void content composites always exhibited higher tan$\delta$ than low void content composites. A possible cause is that the non-affine deformation of the copper skeleton is restrained more when additional metal filler is introduced

Non-linearities in the composite properties with respect to the strain level were observed. Higher strain level resulted in lower loss tangent, and lower modulus for the composite of conventional copper foam and solder, as shown in Figure 12. A significant increase in the loss tangent at low frequencies was also observed when the strain level was beyond the yield point for indium (which yields at a very low strain), as shown in

Figure 13. For all other experiments, the strain was kept well below the yield point by controlling the input torque.


## STIFFNESS-LOSS MAPS: INTERPRETATION

Viscoelastic properties of composites corresponding to the Voigt, Reuss, and Hashin-Shtrickman bounds on the elastic moduli (for given volume fraction of one phase) have been determined in a companion article. Such 'bounds' enclose a region on a stiffness-loss map, however we do not yet know if they represent bounds upon viscoelastic properties. Nevertheless, they represent physically realizable composites and we display them with the experimental results for the purpose of comparison.

Figures 14-17 show stiffness-loss maps based on measured viscoelastic properties for copper foams and low void content composites at 1 kHz, along with theoretical plots for Voigt, Reuss, and Hashin composites. The Voigt and Reuss curves embody the assumption of only two phases, both solid, hence no voids. The effect of voids in composites with copper, filler, and small pores was incorporated via the multi-phase Hashin composite analysis.

Viscoelastic properties of copper foam with no filler are shown in Figure 14. The loss tangent substantially exceeds that of pure copper at the higher frequencies. This observation is at variance with theory which indicates the loss tangent of a solid is not altered by the presence of voids (Christensen, 1969). That theory agrees with the Voigt curve in Figure 14. The Reuss curve, however gives a nonzero stiffness in the presence of voids. This is initially surprising, since in the purely elastic Reuss case one constituent of stiffness tending to zero results in a composite with stiffness which tends to zero. However, in the present analysis the 'void' phase was given a small loss which contributes to $|G^*|$. The Voigt and Reuss curves in Figure 14 were generated by assuming a 'filler' of small stiffness and loss which were then allowed to tend to zero. The shape of the curves in the vicinity of the point representing the stiff constituent was insensitive to the ratio of stiffness to loss of the 'void' phase during the limiting procedure. The relatively high tanδ experimentally obtained most likely arises from physical processes not included in the elementary analysis. The frequency is too low for viscosity due to air moving in the foam pores to contribute much to the loss, but surface effects in the copper or losses due to cold work may be of interest.

Viscoelastic results of the copper-viscoelastic elastomer composites shown in Figure 15 lie within the region formed by the Voigt and Reuss curves. Figure 16 shows the results of the low void content solder filler foams. For the re-entrant copper foam-

solder composite, the experimentally obtained result is close to the data point predicted by the upper Hashin curve; the loss for the conventional copper foam composite is somewhat lower. Figure 17 shows the results of the low void content indium filler composite. Similar results are found as those for the solder filler composites shown in Figure 16. The composite with re-entrant copper foam has results closer to the upper Hashin curve than that with conventional copper composite.

The composites examined in this study all substantially exceeded the (lower) Voigt and Hashin curves in the stiffness loss map, hence they performed better (in combining stiffness and loss) than would a composite containing spherical compliant inclusions (Chen and Lakes, submitted). The composites with two metal phases approached the upper Hashin curve computed allowing for the residual porosity. It is likely that the difference between the metal-polymer composite and the metal-metal composites arises from the degree of restraint on the non-affine unfolding of the copper skeleton, which depends on the stiffness of the filler. None of the composites examined here is as stiff as we would like in a structural material. The reason is that the volume fraction of the stiff constituent was in all cases small. Nevertheless they have served as model materials to illustrate the effect of non-affine deformation in composites made with negative Poisson's ratio foam. Among the 'homogeneous' materials a magnetic ferrite displayed a good combination of stiffness and loss, as shown in Table 2 and Fig. 18. It may be of interest to incorporate such ferrites in future high-loss composites.

## CONCLUSIONS

1. A viscoelastic elastomer exhibited high loss at high frequency and two high loss metals, solder and indium, exhibited high loss at low frequency and comparatively high loss at high frequency.

2. Viscoelastic properties of copper-viscoelastic elastomer composites exceeded the (lower) Voigt limit. Composite based on re-entrant foam exhibited a higher loss than one based on conventional foam.

3. Composites of copper foam and indium or solder exhibited losses close to the Hashin three phase upper bound with the third phase being pore space.

## ACKNOWLEDGMENT

# REFERENCES

Ashby, M.F., (1983), "The mechanical properties of cellular solids", *Metallurgical transactions A,* **14A,** 1755-1769.

Choi, J. B. and Lakes, R. S., (in press), "Nonlinear properties of polymer cellular materials with a negative Poisson's ratio", *J. Materials Science,* accepted (1991).

Chen, C.P. and Lakes, R.S., (submitted) "Analysis of high loss viscoelastic composites".

Chen, C.P. and Lakes, R.S., (1989)"Dynamic wave dispersion and loss properties of conventional and negative Poisson's ratio polymeric cellular materials", *Cellular polymers,* **8** , 343-359.

Chen, C.P. and Lakes, R.S., (1989), "Apparatus for determining the viscoelastic properties of materials over ten decades of frequency and time", *J. Rheology,* **33(8),** 1231-1249.

Chen, C.P. and Lakes, R.S., (1991) "Holographic study of conventional and negative Poisson's ratio metallic foams: elasticity, yield, and micro-deformation", J. Materials Science **26,** 5397-5402.

Christensen, R.M., *Theory of viscoelasticity,* 2nd ed., Academic Press, New York, 1982.

Christensen, R.M., (1969), "Viscoelastic properties of heterogeneous media", *J. Mech. Phys. Solids,* **17** 23-41.

Ferry, J.D., *Viscoelastic properties of polymers,* 2nd ed., Wiley, New York, 1970.

Lakes, R.S. (1987),"Foam structures with a negative Poisson's ratio", *Science,* **235,** 1038-1040 .

Lakes, R.S. (1991), "Deformation mechanisms of negative Poisson's ratio materials: structural aspects", *J. Materials Science,* **26,** 2287-2292.

Lakes, R.S., Katz, J.L., and Sternstein, S.S., (1979), "Viscoelastic properties of wet cortical bone: Part I, torsional and biaxial studies." *Journal of Biomechanics,* **12,** 657-678.

Nielsen, I., *Mechanical Properties of Polymers,* Reinhold, 1962.

Nowick A. S. and Berry, B. S.*Anelastic relaxation in crystalline solids,* Academic, N.Y., 1972.

Shipkowitz, A.T., Chen, C.P. and Lakes, R.S., (1988), "Characterization of high-loss viscoelastic elastomers", *J. Materials Science,* **23,** 3660-3665.

Smithells, C.J., *Metals reference book,* 5th ed., Butterworths, London and Boston, 1976.

## TABLE 1 Specimen dimensions

| Material | Width(mm) | Length(mm) |
|---|---|---|
| Elastomer | 6.35 dia | 2.7 |
| Solder | 3.125 dia | 228.5 |
| Indium | 1.0 dia | 13 |
| Gallium | 1.6 dia | 11 |
| Copper | 0.85 dia | 65 |
| Brass | 1.1 dia | 30 |
| Ferrite, non mag | 0.95 square | 13.5 |
| Ferrite, magnetic | 0.95 square | 15 |
| Composite, conventional Cu-elastomer | 6.4 square | 40 |
| Composite, re-entrant Cu-elastomer | 5.4 by 6.9 | 41 |
| Composite, conventional Cu-solder | 5.55 square | 38.5 |
| Composite, re-entrant Cu-solder | 4.2 by 4.6 | 31.1 |
| Composite, conventional Cu-indium | 4.9 square | 36 |
| Composite, re-entrant Cu-indium | 4.6 | 25 |

**TABLE 2** Viscoelastic properties of solid materials and foams

| Materials | Volumetric fraction | 0.1 Hz Shear Modulus \|G*\| ( GPa ) | loss tangent tanδ | 1 kHz Shear Modulus \|G*\| ( GPa ) | loss tangent tanδ |
|---|---|---|---|---|---|
| Solid copper | 100% | 40. | ≅0.0001 | 40. | ≅0.002 |
| Solid brass | 100% | | | 24 | 0.0012 |
| Conventional copper foam | Copper: 7.61% | 0.0356 | ≤0.012 | 0.043 | 0.0068 |
| Re-entrant copper foam | Copper: 11.3% | 0.0268 | ≤0.012 | 0.0391 | 0.0134 |
| Polymer(elastomer) | 100% | 0.000131 | 0.14 | 0.00136 | 0.79 |
| Solder | 100% | 9.73 | 0.0472 | 13.8 | 0.018 |
| Indium | 100% | 2.82 | 0.095 | 4.27 | 0.025 |
| Gallium | 100% | 12.6 | 0.031 | 16.5 | 0.033 |
| Ferrite, magnetic | 100% | 28.8 | ≤0.012 | 32.1 | 0.055 |
| Ferrite, nonmagnetic | 100% | 30 | ≤0.012 | 30.5 | 0.021 |

**TABLE 3** Viscoelastic properties of composite materials

| Materials | Volumetric fraction | 0.1 Hz | | 1 kHz | |
|---|---|---|---|---|---|
| | | Shear Modulus \|G*\| ( GPa ) | loss tangent tanδ | Shear Modulus \|G*\| ( GPa ) | loss tangent tanδ |
| Conventional copper foam + Polymer | Copper: 7.61% Polymer: 76.1% | 0.0712 | ≤0.012 | 0.0925 | 0.056 |
| Re-entrant copper foam + Polymer | Copper: 11.3% Polymer: ≈100% | 0.0466 | ≤0.012 | 0.0838 | 0.167 |
| Conventional copper foam + Solder | Copper: 7.61% Solder: 22.1% | 0.121 | ≤0.012 | 0.121 | 0.02 |
| Re-entrant copper foam + Solder | Copper: 11.3% Solder: 33.6% | 0.263 | 0.0157 | 0.284 | 0.0366 |
| Conventional copper foam + Solder | Copper: 7.61% Solder: 79.9% | 9.28 | 0.0157 | 11.0 | 0.0112 |
| Re-entrant copper foam + Solder | Copper: 11.3% Solder: 77.7% | 11.9 | 0.0157 | 13.5 | 0.013 |
| Conventional copper foam + Indium | Copper: 7.61% Solder: 23.4% | 0.560 | 0.0314 | 0.639 | 0.0519 |
| Re-entrant copper foam + Indium | Copper: 11.3% Solder: 12. % | 0.103 | ≤0.012 | 0.115 | 0.021 |
| Conventional copper foam + Indium | Copper: 7.61% Solder: 78.5% | 2.89 | 0.0472 | 3.57 | 0.0144 |
| Re-entrant copper foam + Indium | Copper: 11.3% Solder: 74.7% | 4.93 | 0.0157 | 5.58 | 0.0149 |

## List of figures

1. Viscoelastic behavior of copper foams. ☐ and ◊: Conventional copper foam (volumetric fraction: 7.61%), Go = G(0.1Hz) = 0.0356 GPa. ■ and ♦: Re-entrant. copper foam (volumetric fraction: 11.3%), Go = G(0.1Hz) = 0.0268 GPa.

2. Viscoelastic behavior of viscoelastic elastomer polymer. Go = G(0.1Hz) = 0.000131 GPa.

3. Viscoelastic behavior of composite of copper foams and polymer filler. ☐ and ◊: Conventional copper foam and polymer (volumetric fraction: 76.1%), Go = G(0.1Hz) = 0.0714 GPa. ■ and ♦: Re-entrant. copper foam and polymer (volumetric fraction: ≈100%), Go = G(0.1Hz) = 0.0466 GPa.

4. Viscoelastic behavior of solder. Go = G(0.1Hz) = 9.73 GPa.

5. Viscoelastic behavior of composite of copper foams and large void content solder filler. ☐ and ◊: Conventional copper foam and solder (volumetric fraction: 22.1%), Go = G(0.1Hz) = 0.121 GPa. ■ and ♦: Re-entrant. copper foam and solder (volumetric fraction: 33.6%), Go = G(0.1Hz) = 0.263 GPa.

6. Viscoelastic behavior of composite of copper foams and low void content solder filler. ☐ and ◊: Conventional copper foam and solder (volumetric fraction: 79.9%), Go = G(0.1Hz) = 9.28 GPa. ■ and ♦: Re-entrant. copper foam and solder (volumetric fraction: 77.7%), Go = G(0.1Hz) = 11.87 GPa.

7. Viscoelastic behavior of indium. Go = G(0.1Hz) = 2.82 GPa.

8. Viscoelastic behavior of composite of copper foams and large void content indium filler. ☐ and ◊: Conventional copper foam and indium (volumetric fraction: 23.4%), Go = G(0.1Hz) = 0.56 GPa. ■ and ♦: Re-entrant. copper foam and indium (volumetric fraction: 12%), Go = G(0.1Hz) = 0.103 GPa.

9. Viscoelastic behavior of composite of copper foams and low void content indium filler. ☐ and ◊: Conventional copper foam and indium (volumetric fraction: 78.5%), Go = G(0.1Hz) = 2.89 GPa. ■ and ♦: Re-entrant copper foam and indium (volumetric fraction: 74.7%), Go = G(0.1Hz) = 4.93 GPa.

10. Stiffness-loss map of viscoelastic behavior of matrix, fillers, and composites at 0.1 Hz.

11. Stiffness-loss map of viscoelastic behavior of matrix, fillers, and composites at 1 kHz.

12. Nonlinearity of 1st resonant frequency and loss tangent tanδ with respect to strain level. Conventional copper foam matrix and large void content solder composite, ≈ 1kHz.

13. Nonlinearity of shear modulus $|G^*|$ and loss tangent tan$\delta$ with respect to strain level. Indium, 0.1 Hz.

14. Stiffness-loss map of copper and copper foams. ▢ : experimental data for conventional copper foam. Δ: experimental data for re-entrant copper foam. Idealized composites of copper foams at 1 kHz. x: Voigt composite, +: Reuss composite.

15. Stiffness-loss map of copper and composites containing copper foam and viscoelastic elastomer polymer. Idealized composites of copper foams and polymer filler at 1 kHz. x: Voigt composite, +: Reuss composite, ◊: upper bound of three-phase Hashin composite with 16.3% voids included. ▢ : experimental data of conventional copper foam matrix composite. Δ: experimental data of re-entrant copper foam matrix composite.

16. Stiffness-loss map of copper and composites containing copper foam and solder. Idealized composites of copper foams and low void content solder filler at 1 kHz. x: Voigt composite, +: Reuss composite, ◊: upper bound of three-phase Hashin composite with 11% voids included. ▢ : experimental data of conventional copper foam matrix composite. Δ: experimental data of re-entrant copper foam matrix composite.

17. Stiffness-loss map of copper and composites containing copper foam and indium. Idealized composites of copper foams and low void content indium filler at 1 kHz. x: Voigt composite, +: Reuss composite, ◊: upper bound of three-phase Hashin composite with 14% voids included. ▢ : experimental data of conventional copper foam matrix composite. Δ: experimental data of re-entrant copper foam matrix composite.

18 Stiffness-loss map of several materials including solid materials examined in this study.

   Steel, 1 Hz, after Nowick and Berry (1972)

   Copper, 600 Hz, after Nowick and Berry (1972)

   Polymethyl methacrylate, (PMMA), 10 Hz and 1 kHz, after Ferry (1979)

   Bone, 1-100 Hz, after Lakes, Katz, Sternstein (1979)

   Hevea rubber, 10 Hz-2 kHz, after Ferry (1979)

   Polystyrene, 100 Hz, 1kHz, after Ferry (1979)

   Polycarbonate, 100 Hz, after Nielsen (1962)

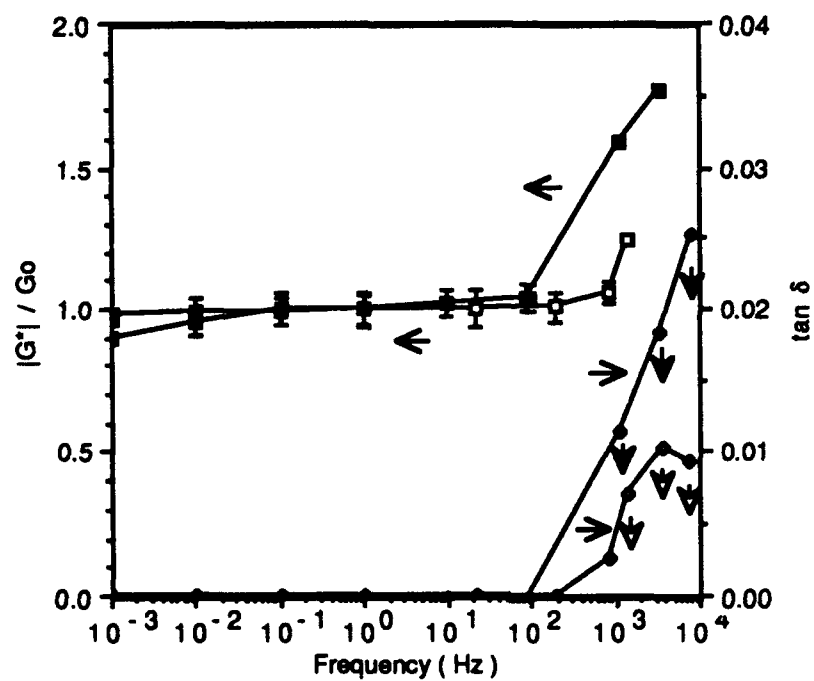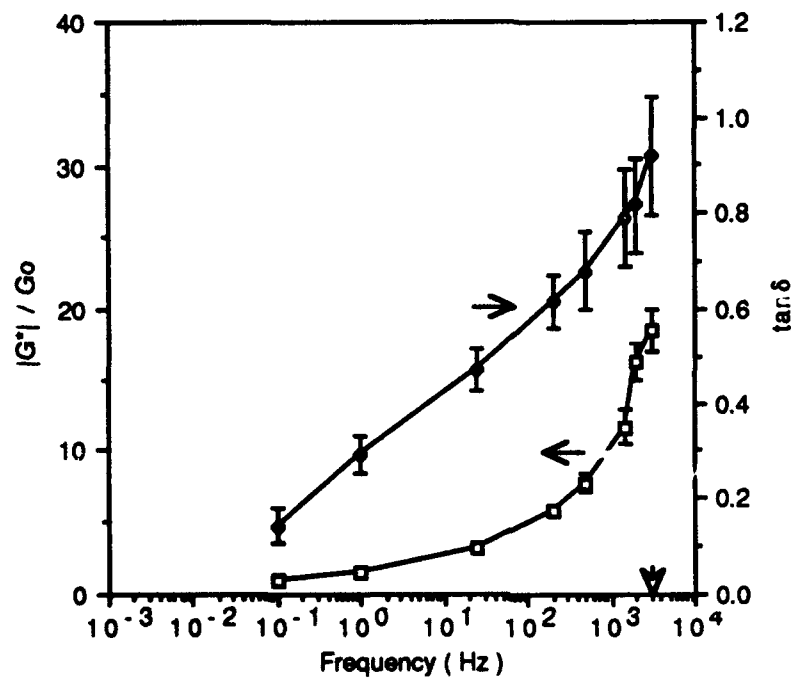   Viscoelastic elastomer, 100, 1,000 Hz, after Shipkowitz, et. al. (1988)

Fig. 1

Chem, lakes - Cu foam

Fig. 2
Chen, Lakos
-polymer

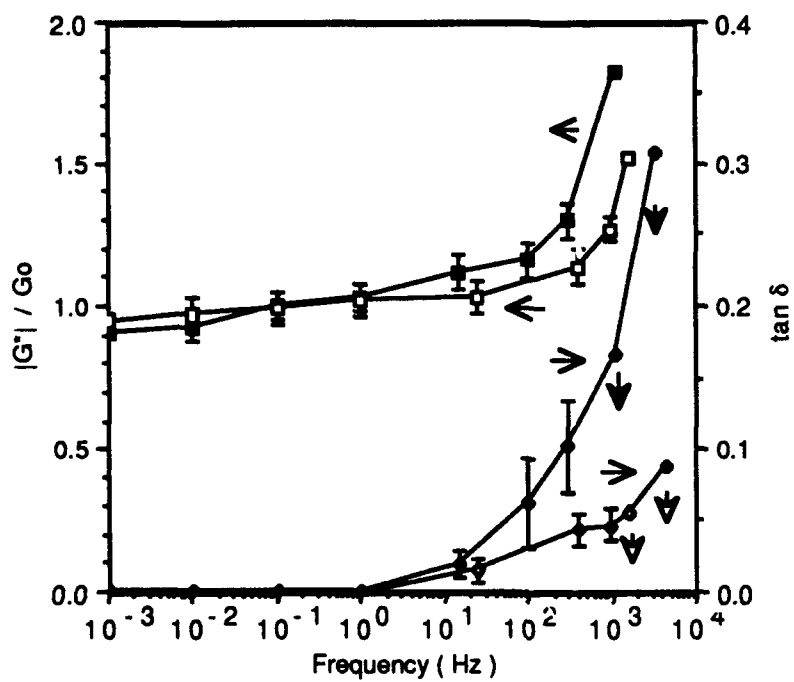2  POLYMER

Fig. 3
Chen, Latex
Cu-Polymer
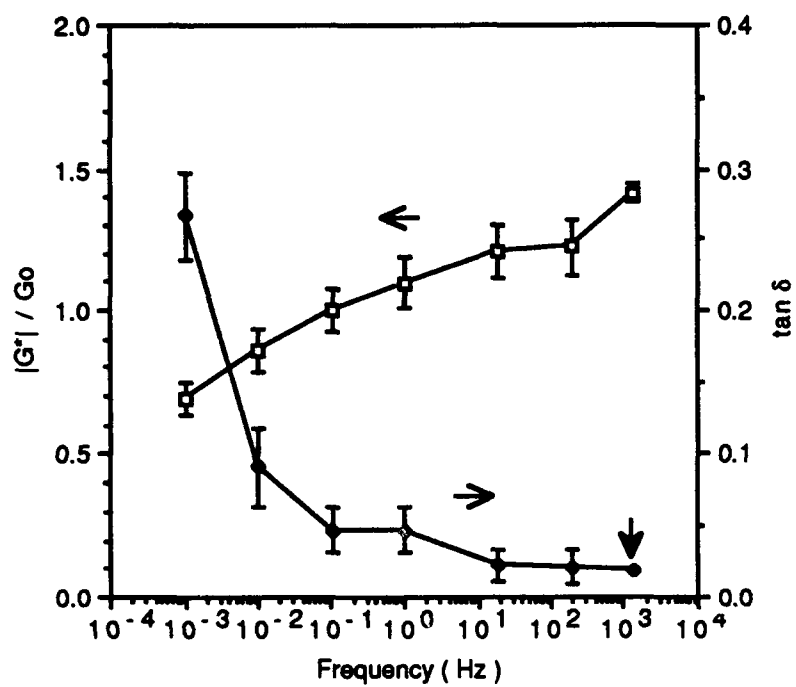
Fig. 4
Chen, Inbar
Solder
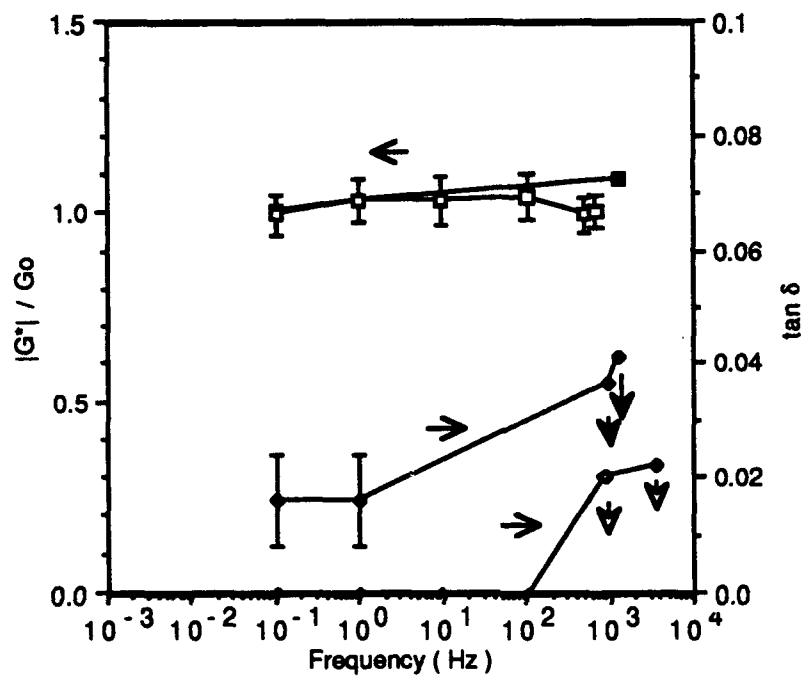
Fig. 5
Chen, Laios
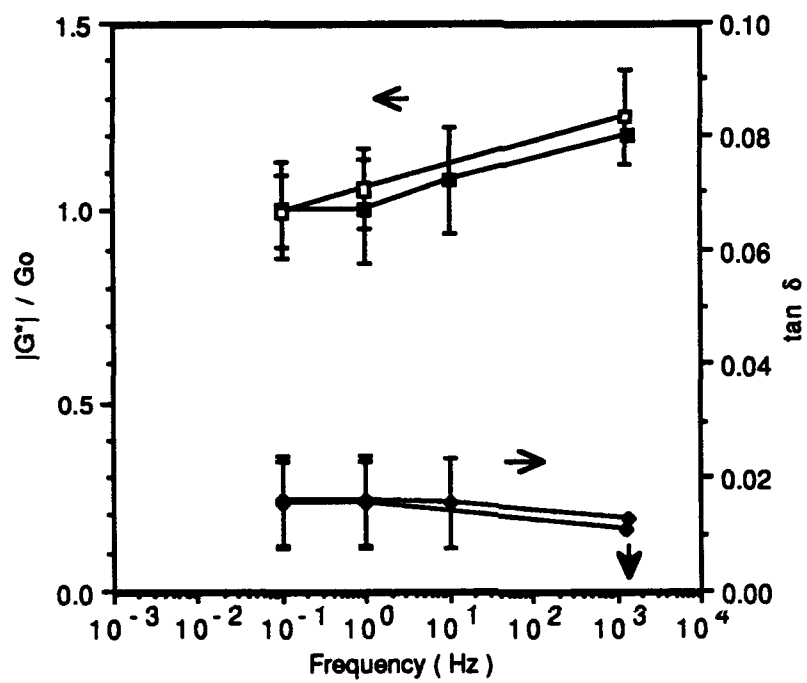(n-solder-void)

Fig. 6
Chen, Lakes
Cu-Solder
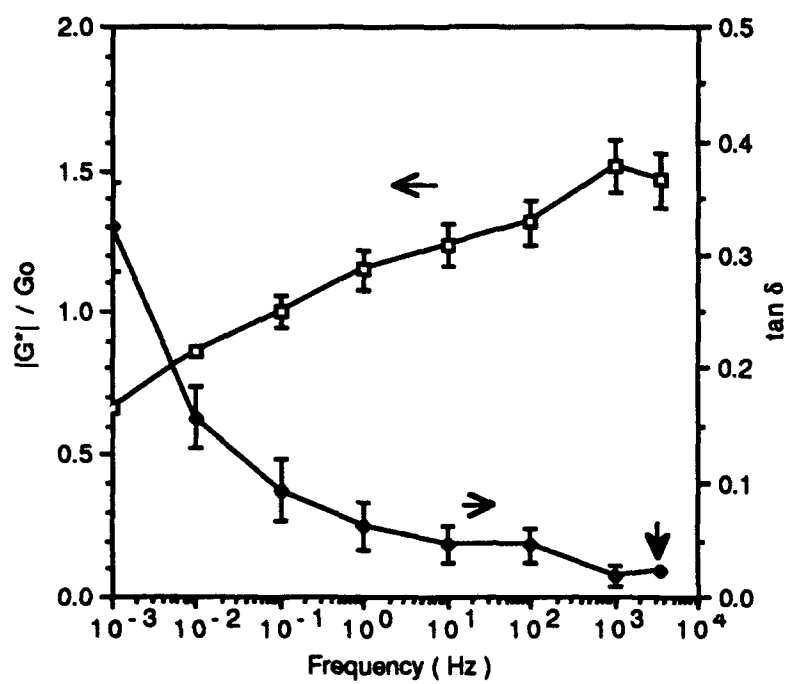
Fig. 7
rheology
Indium
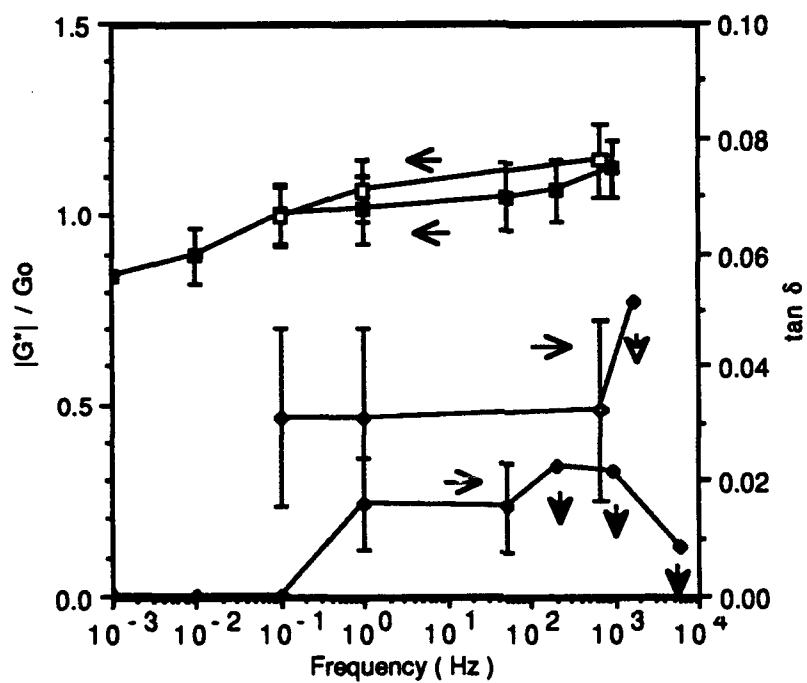
Fig. 8
Chen, Labes
Cn-indium-bonds
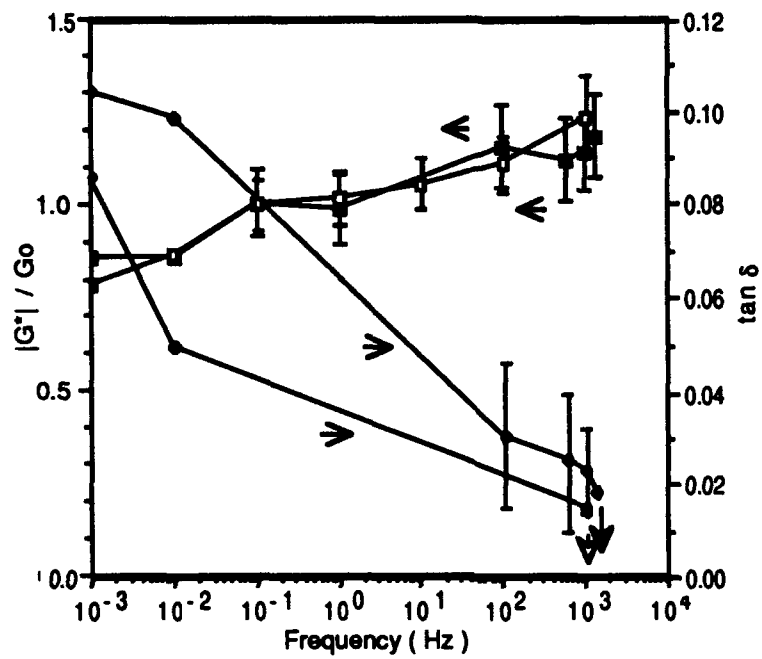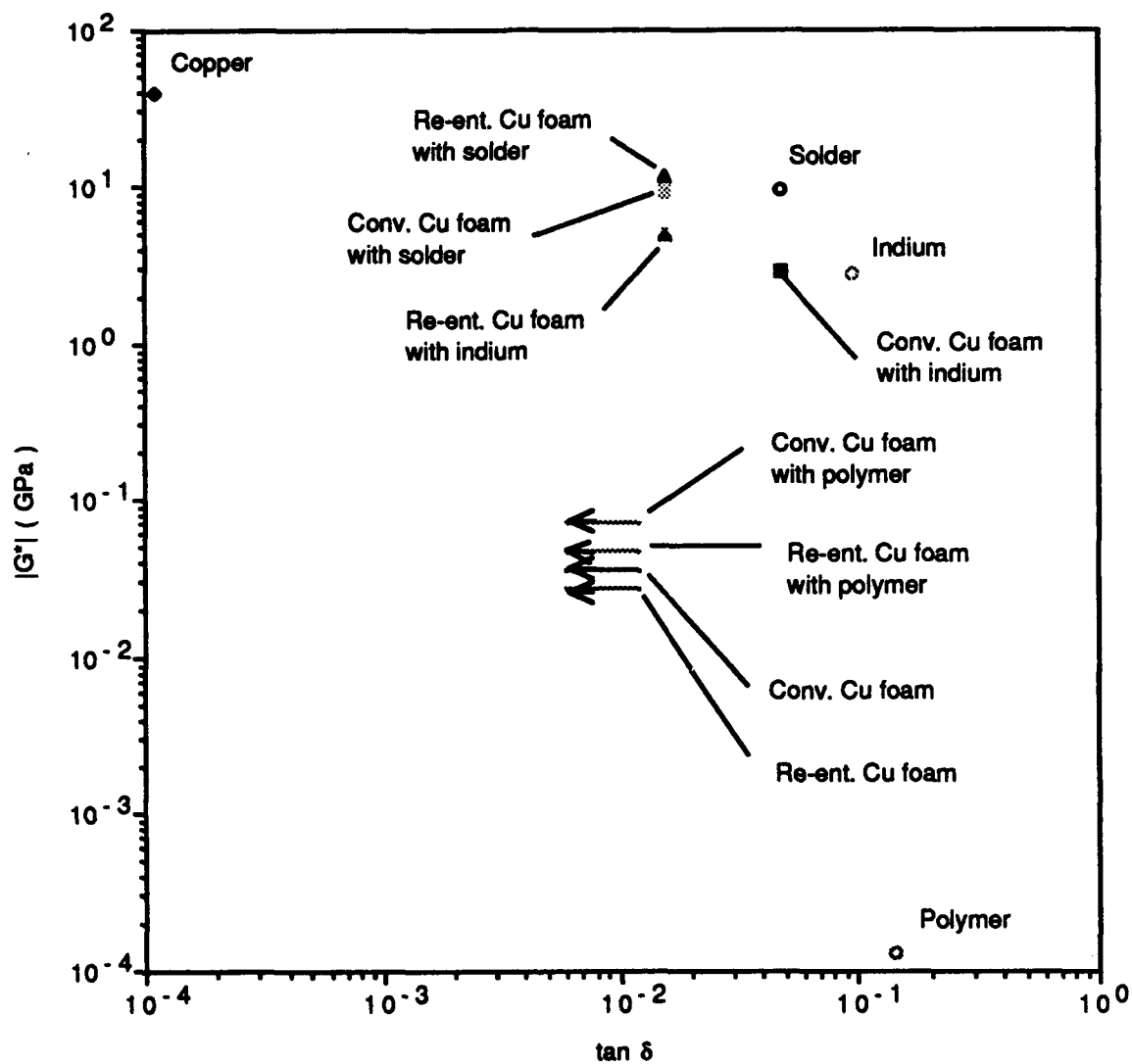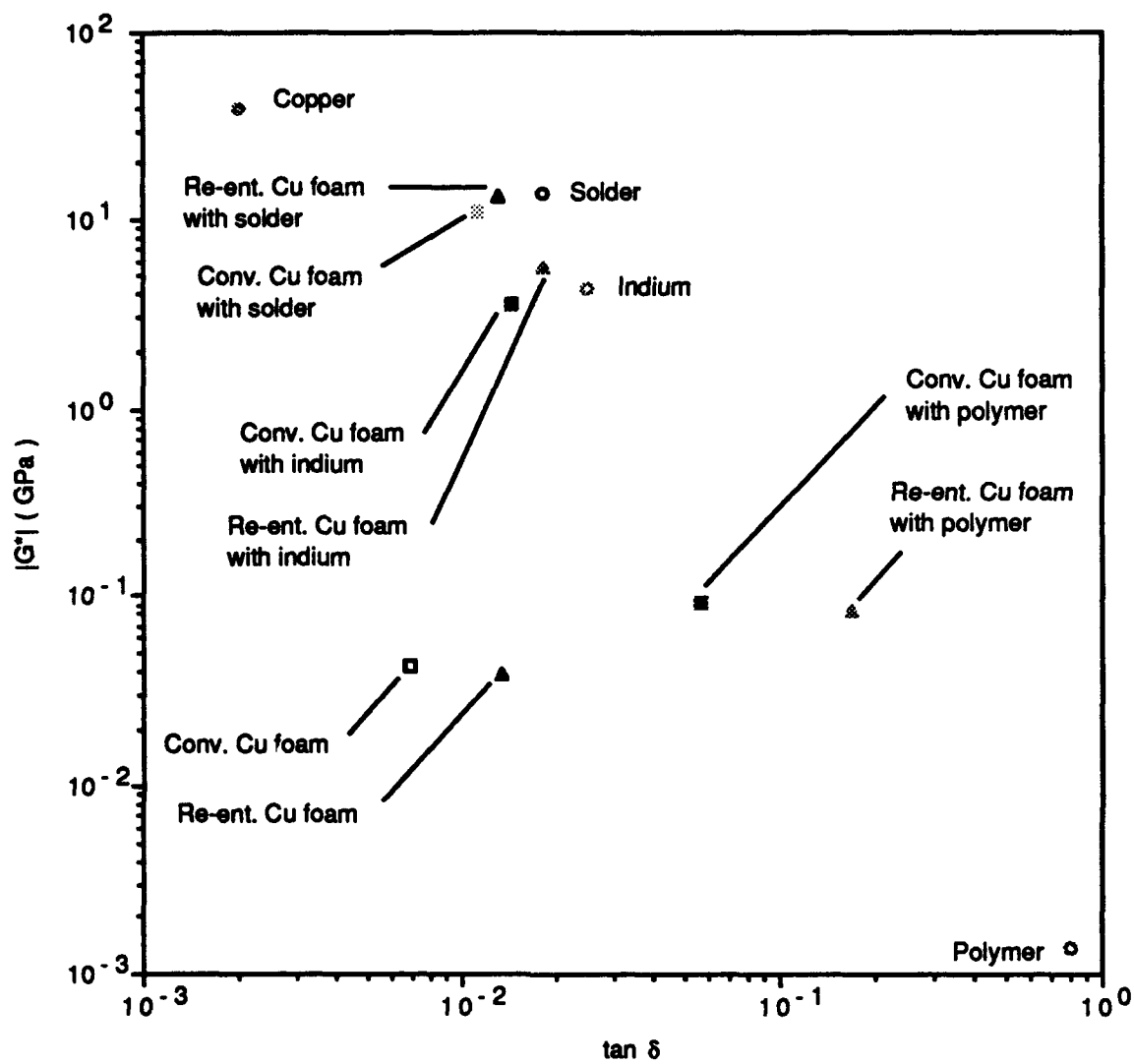
Fig 7
Chen, labs
Cu - indium

Copper

Re-ent. Cu foam
with solder

Conv. Cu foam
with solder

Re-ent. Cu foam
with indium

Solder

Indium

Conv. Cu foam
with indium

Conv. Cu foam
with polymer

Re-ent. Cu foam
with polymer

Conv. Cu foam

Re-ent. Cu foam

Polymer

$|G^*|$ ( GPa )

$10^2$
$10^1$
$10^0$
$10^{-1}$
$10^{-2}$
$10^{-3}$
$10^{-4}$

$10^{-4}$  $10^{-3}$  $10^{-2}$  $10^{-1}$  $10^0$

tan δ

Fig. 10
Chen, Lakes
M.P., 0.1 Hz

Fig. 11
Chen, lakes
Map, 1kHz

Fig 12
than inter
Cu-solder-iron

Shear strain ( % )

Fig 13.
Chan, Kros
Indian J. ...

Reuss
Copper: 99.99999999%

Copper

Voigt
Copper: 50%

Experiment
Conv. Cu foam

Experiment
Re-ent. Cu foam

$|G^*|$ ( GPa )

$10^3$

$10^2$

$10^1$

$10^0$

$10^{-1}$

$10^{-2}$

$10^{-3}$

$10^{-2}$

$10^{-1}$

tan δ

Fig. 4
Chen et al.
Cu – 1kHz

Fig. 15
cur, lates
map, 1 kHz

Fig-16

Voigt
Copper: 90%

Reuss
Copper: 75%

Copper

$|G^*|$ ( GPa )

3 phase Hashin
Copper: 15%
Indium: 71%

Indium

3 phase Hashin
Copper: 10%
Indium: 76%

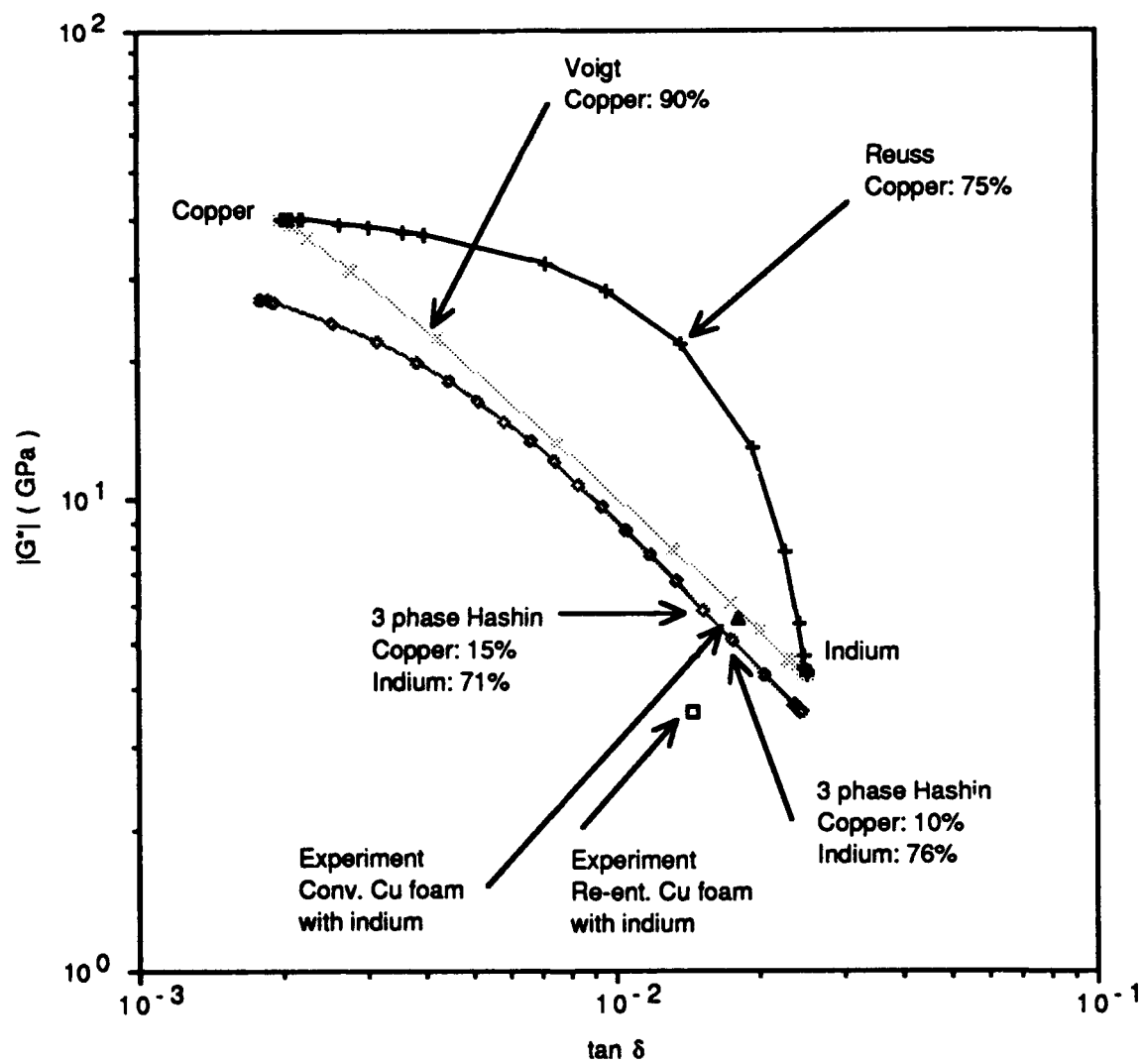Experiment
Conv. Cu foam
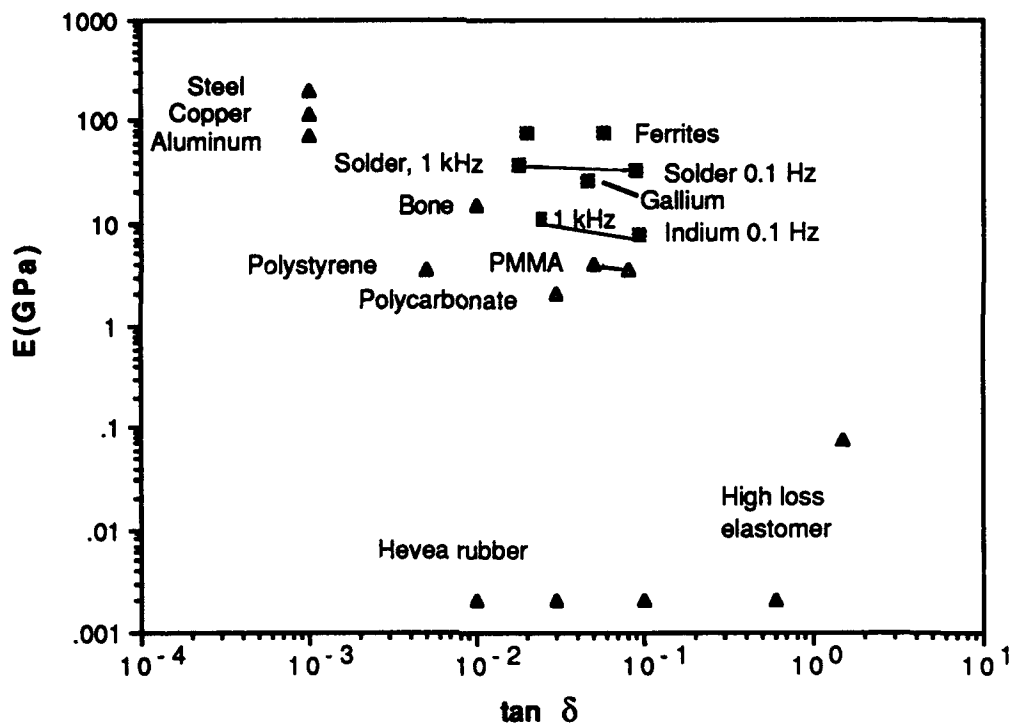with indium

Experiment
Re-ent. Cu foam
with indium

tan δ
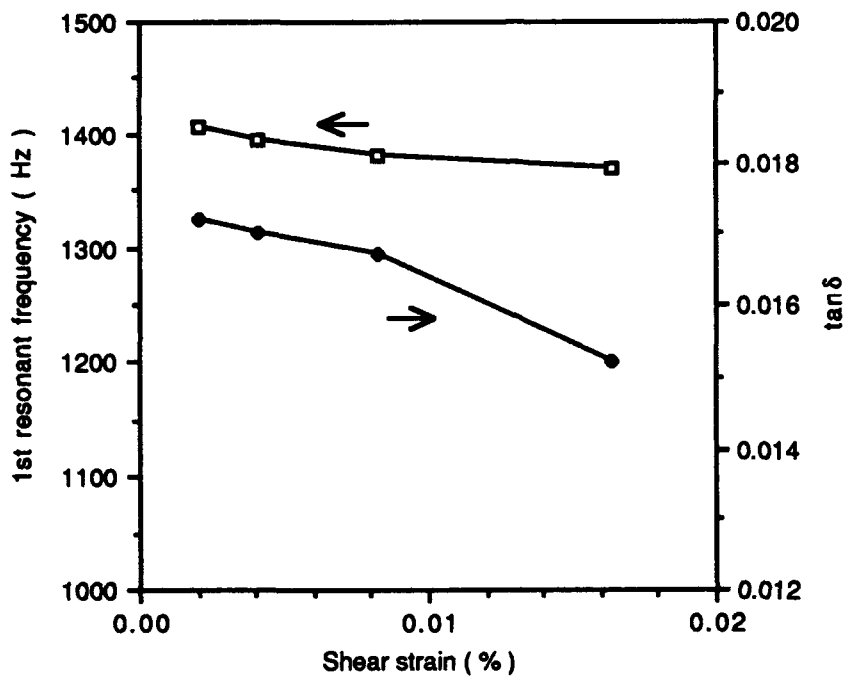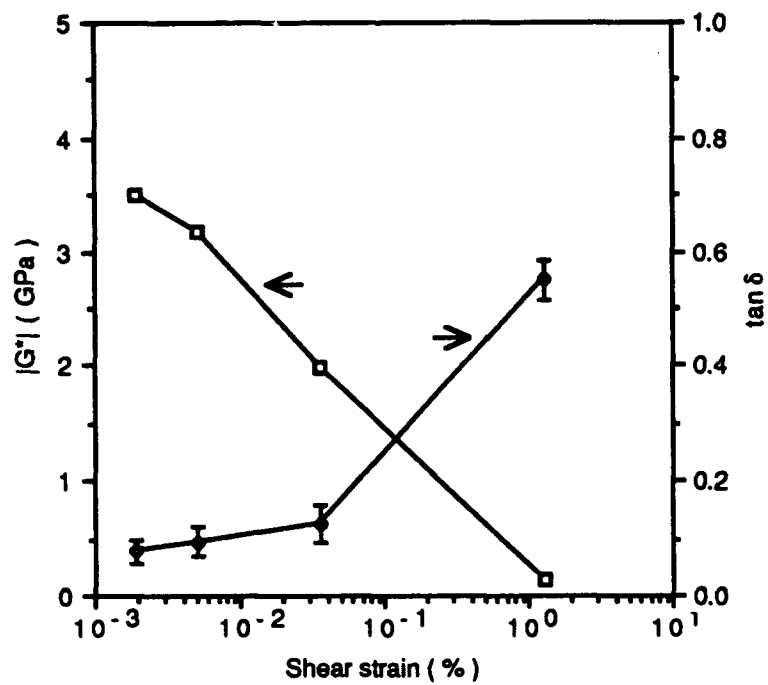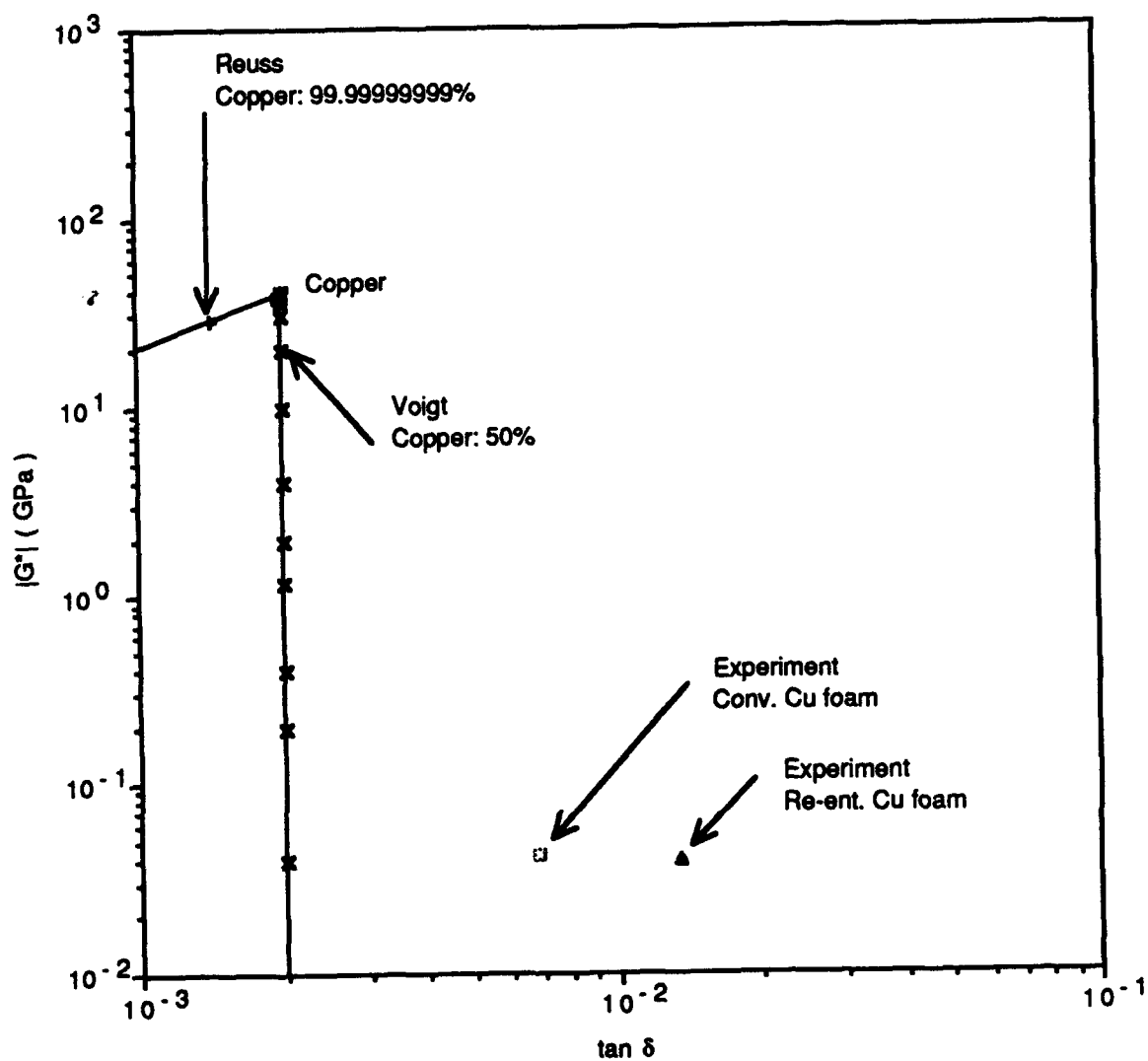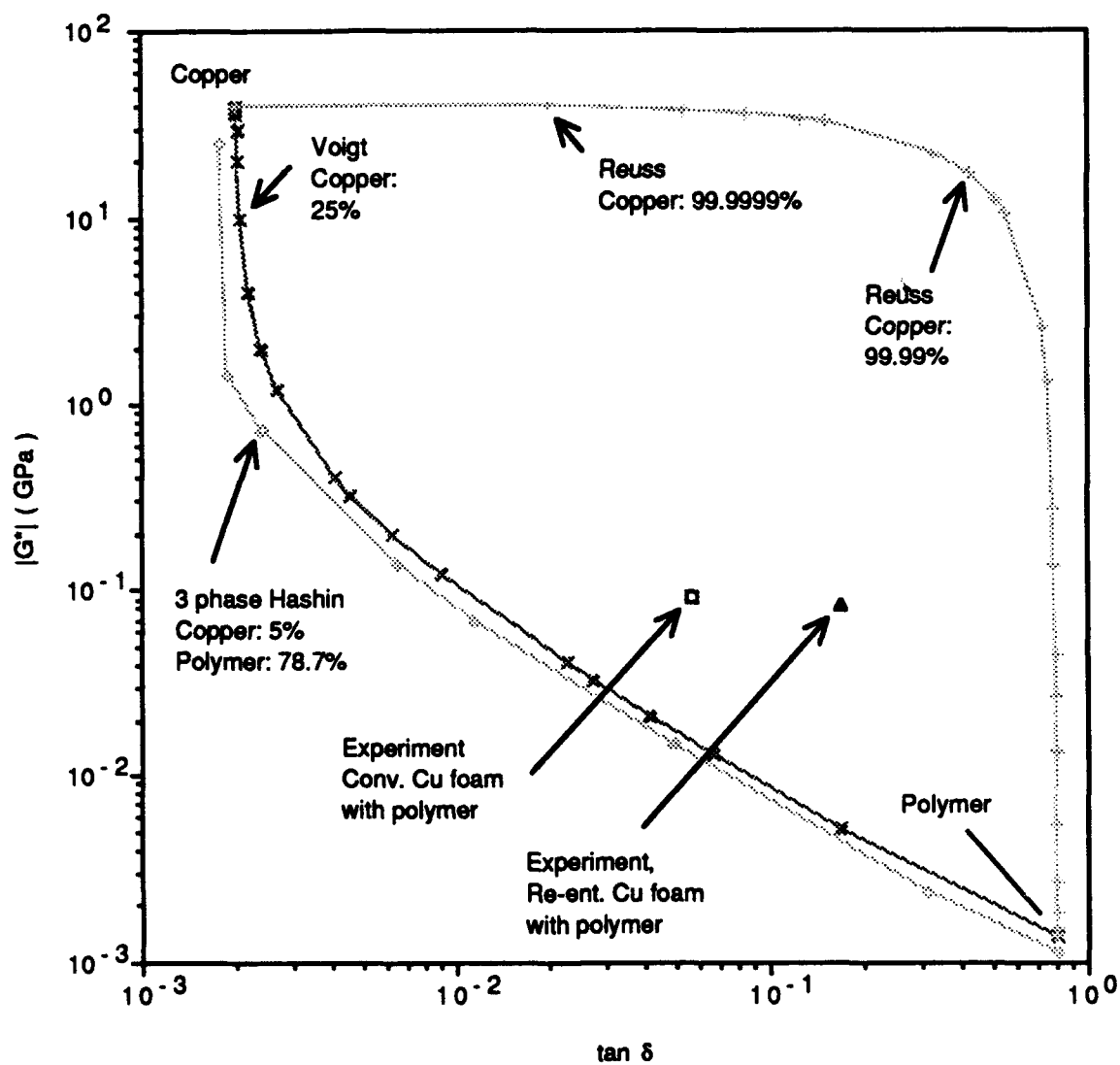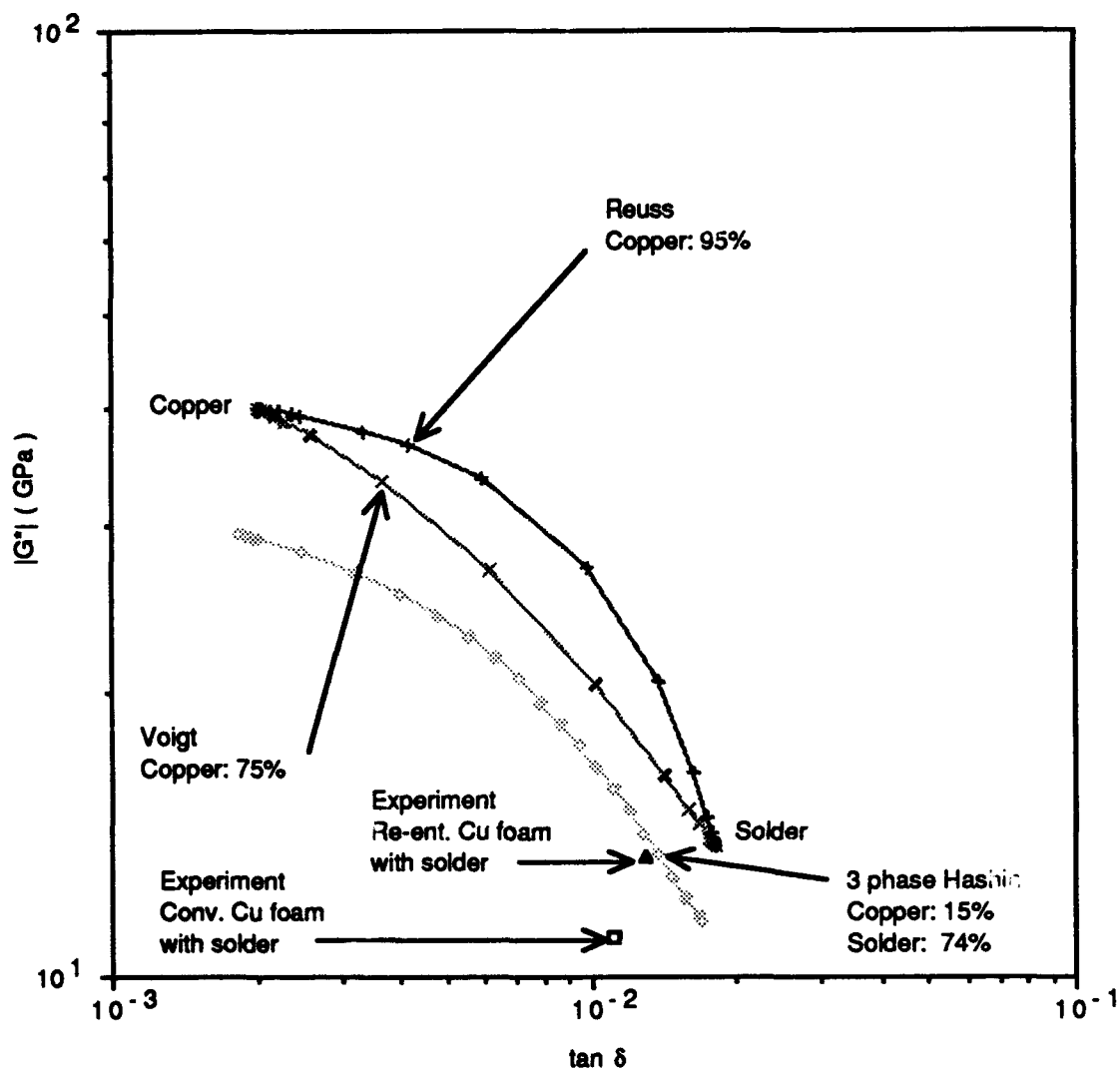
Fig 18
Clarke's

# Analysis of high loss viscoelastic composites

by

C. P. Chen*, Ph.D., Postdoctoral researcher

and

R. S. Lakes§, Ph.D., Professor


*§Department of Mechanical Engineering

§Department of Biomedical Engineering

§Center for Laser Science and Engineering

University of Iowa

Iowa City, IA 52242


§ Address correspondence to R. Lakes

28 July 1991

Revised 2 May 1992

## Synopsis

A theoretical study of viscoelastic properties of composites is presented with the aim of identifying structures which give rise to a combination of high stiffness and high loss tangent. Laminates with Voigt and Reuss structure, as well as composite materials attaining the Hashin-Shtrickman bounds on stiffness were evaluated via the correspondence principle. Similarly, viscoelastic properties of composites containing spherical or platelet inclusions were explored. Reuss laminates and platelet filled materials composed of a stiff, low loss phase and a compliant high loss phase were found to exhibit high stiffness combined with high loss tangent.

# INTRODUCTION

Viscoelastic materials can be of use in the damping of mechanical vibration and in the absorption of sound. The loss tangent, or tangent of the phase angle $\delta$ between stress and strain in sinusoidal loading, is a useful measure of material damping. Most materials used in structural applications, however, have small loss tangents. Conversely, materials with high loss tangents tend to be compliant, hence not of structural interest. Fig. 1 contains a stiffness-loss map (plot of the absolute value of the dynamic modulus vs loss tangent) for some representative materials. Compliant, lossy materials are used as layers over stiff materials in various applications; nevertheless a stiff material with high loss would be of use in structural damping of noise and vibration. We consider in this article the possibility of making composite microstructures providing high stiffness and high loss.

A possible avenue for making high loss composites is to make use of non-affine deformation. This is in contrast to affine deformation in which the particles in the solid move in a way corresponding to a uniform strain plus a rotation in a continuum. The negative Poisson's ratio materials developed by Lakes (1987) exhibit this property in that the foam cells unfold during deformation (Lakes, 1991; Chen and Lakes, 1991). Non-affine deformation can result in high viscoelastic loss in a composite if the phase which has the highest loss experiences a larger strain than does the composite as a whole.

Elastic properties of multi-phase composite materials have been studied extensively. Of these studies, the ones most relevant to the present work are those dealing with bounds on the elastic behavior and predicted properties of composites of relatively simple structure. The upper and lower bounds of stiffness of two phase and many phase

composite materials have been obtained in terms of volume fraction of constituents(Hashin, 1962; Hashin and Shtrickman, 1963). Bounds and expressions for the effective elastic moduli of materials reinforced by parallel hollow circular fibers in hexagonal or random arrays have also been derived by a variational method (Hashin, 1962). Furthermore, bounds on three independent effective elastic moduli of an n-phase fiber reinforced composite of arbitrary transverse phase geometry, plane strain bulk modulus, transverse shear modulus and shear modulus in plane parallel to fibers, have been derived in terms of phase volume fractions(Hashin, 1965a). For viscoelastic heterogeneous media of several discrete linear viscoelastic phases with known stress-strain relations, it was shown that the effective relaxation and creep functions could be obtained by the correspondence principle of the theory of linear viscoelasticity (Hashin, 1965b). In some cases explicit results in terms of general linear viscoelastic matrix properties was given, and thus permitting direct use of experimental information (Hashin, 1966). In a review by Ahmed and Jones (1990) of particulate reinforcement theories for polymer composites, it was concluded that the macroscopic behavior was affected by the size, shape, distribution, and interfacial adhesion of the inclusions. This article makes use of some of these results for elastic composites to explore accessible regions of the stiffness-loss maps of the materials.

## ELASTIC AND VISCOELASTIC PROPERTIES OF COMPOSITES

For the simplest case of a two-phase composite, the Voigt and Reuss composites described below represent rigorous upper and lower bounds on the Young's modulus for a given volume fraction of one phase. The Hashin-Shtrickman composites represent upper and lower bounds for isotropic elastic composites. Viscoelastic composites containing spherical or platelet inclusions are also considered. Results obtained via the correspondence principle are plotted as "stiffness-loss maps" in the subsequent section.

### Voigt composite

Let phase 1 be stiff; let phase 2 be high loss. The geometry of the Voigt model structure is shown in Figure 2. The composite can contain laminations as shown in Figure 1(a) or it can be made of continuous fibers in Figure 1(b); in either case the strain in each phase is the same. For an elastic material with one of these structures, the Voigt relation is

$$E_c = E_1 V_1 + E_2 V_2,$$

in which $E_c$, $E_1$ and $E_2$ refer to the Young's modulus of the composite, phase 1 and phase 2, and $V_1$ and $V_2$ refer to the volume fraction of phase 1 and phase 2 with $V_1 + V_2 = 1$. The

Voigt relation for the stiffness of an elastic composite is obtained by recognizing that for the given geometry, the strain in each phase is the same; the forces in each phase are additive.

By the correspondence principle (Hashin, 1970, Christensen, 1980), the elastic relation can be converted to a steady state harmonic viscoelastic relation by replacing the Young's moduli E by $E^*(i\omega)$ or $E^*$, in which $\omega$ is the angular frequency of the harmonic loading. This procedure gives

$$E_c^* = E_1^* V_1 + E_2^* V_2 \qquad (1)$$

with $E^* = E' + i E''$ and loss tangent $\tan\delta = E''/E'$. Taking the ratio of real and imaginary parts, we obtain the loss tangent of the composite $\tan \delta_c = E_c''/E_c'$.

$$\tan \delta_c = \frac{V_1 \tan\delta_1 + V_2 \frac{E_2'}{E_1'} \tan\delta_2}{V_1 + \frac{E_2'}{E_1'} V_2} \qquad (2)$$

## Reuss composite

The geometry of the Reuss model structure is shown in Figure 1(c); each phase experiences the same stress. For elastic materials, $1/E_c = V_1/E_1 + V_2/E_2$. Again using the correspondence principle, the viscoelastic relation is obtained as

$$\frac{1}{E_c^*} = \frac{V_1}{E_1^*} + \frac{V_2}{E_2^*} \qquad (3)$$

Again separating the real and imaginary parts of $E_c^*$, the loss tangent of the composite $\tan \delta_c$ is obtained:

$$\tan \delta_c = \frac{(\tan\delta_1+\tan\delta_2)[V_1+V_2\frac{E_1'}{E_2'}]-(1-\tan\delta_1\tan\delta_2)[V_1\tan\delta_2+V_2\tan\delta_1\frac{E_1'}{E_2'}]}{(1-\tan\delta_1\tan\delta_2)[V_1+V_2\frac{E_1'}{E_2'}]+(\tan\delta_1+\tan\delta_2)[V_1\tan\delta_2+V_2\tan\delta_1\frac{E_1'}{E_2'}]} \qquad (4)$$

## Hashin-Shtrickman composite: arbitrary two-phase geometry

Allowing for 'arbitrary' phase geometry, the upper and lower bounds on the elastic moduli as a function of composition have been developed using variational principles. The lower bound for the shear modulus $G_L$ of the composite was given as (Hashin and Shtrickman, 1963)

$$G_L = G_2 + \cfrac{V_1}{\cfrac{1}{G_1\text{-}G_2} + \cfrac{6(K_2+2G_2)V_2}{5(3K_2+4G_2)G_2}} \qquad (5)$$

in which $K_1$, $G_1$ and $V_1$, and $G_2$ and $V_2$ are the bulk modulus, shear modulus and volume fraction of phases 1, and 2, respectively. Here $G_1 > G_2$, so that $G_L$ represents the lower bound on the shear modulus. Interchanging the numbers 1 and 2 in Equation(5) results in the upper bound $G_U$ for the shear modulus.

As for viscoelastic materials, we again apply the correspondence principle. The complex viscoelastic shear moduli of the composite $G_L^*$ and $G_U^*$ are obtained as

$$G_L^* = G_2^* + \cfrac{V_1}{\cfrac{1}{G_1^*\text{-}G_2^*} + \cfrac{6(K_2^*+2G_2^*)V_2}{5(3K_2^*+4G_2^*)G_2^*}} \qquad (6)$$

and

$$G_U^* = G_1^* + \cfrac{V_2}{\cfrac{1}{G_2^*\text{-}G_1^*} + \cfrac{6(K_1^*+2G_1^*)V_1}{5(3K_1^*+4G_1^*)G_1^*}} \qquad (7)$$

In these cases the loss tangent is more complicated to write explicitly, so it is more expedient to graphically display computed numerical values.

## Hashin transversely isotropic fiber reinforced composites

This case is of interest since it allows more than two phases, a situation applicable to the analysis of experimental results in a companion article. For two phases the results are almost identical to the arbitrary phase geometry case considered above. The shear modulus of elastic multi-phase transversely isotropic fiber reinforced composites of arbitrary transverse phase geometry, can be bounded from below and above in terms of phase moduli and phase volume fractions. The lower and upper bounds on the shear modulus $m^{(-)}$ and $m^{(+)}$ were given for elastic composites (Hashin, 1965a) as

$$m^{(-)} = G_1 + \frac{2G_1(K_1+G_1)}{K_1+2G_1}\left\{\left[\sum_{r=2}^{r=n}\frac{(G_r\text{-}G_1)V_r}{G_1+K_1G_1/(K_1+2G_1)}\right]^{-1}\text{-}1\right\}^{-1} \qquad (8)$$

and

$$m^{(+)} = G_n + \frac{2G_n(K_n+G_n)}{K_n+2G_n}\left\{\left[\sum_{r=1}^{r=n\text{-}1}\frac{(G_r\text{-}G_n)V_r}{G_r+K_nG_n/(K_n+2G_n)}\right]^{-1}\text{-}1\right\}^{-1} \qquad (9)$$

in which n is the number of the phases, $G_1$ and $K_1$ are the shear and bulk moduli of the most compliant phase, $G_n$ and $K_n$ are the shear and bulk moduli of the stiffest phase. r is

a free index representing the phase number; phases are numbered in order of increasing stiffness.

On the basis of the correspondence principle, corresponding results for the complex shear modulus (not necessarily bounds) of the composites are again obtained by replacing $m(-)$, $m(+)$, $G_1$, $K_1$, $G_r$ and $G_n$ by $G_L^*$, $G_U^*$, $G_1^*$, $K_1^*$, $G_r^*$ and $G_n^*$ in Equations(8) and (9), respectively. The loss tangent again is complicated to write explicitly, so it is graphically displayed using computed numerical values.

## Spherical particulate inclusions

For a small volume fraction $V_1 = 1 - V_2$ of spherical elastic inclusions in a continuous phase of another elastic material, the shear modulus of the composite $G_c$ was given as(Christensen, 1979)

$$\frac{G_c}{G_1} = 1 - \frac{15(1-v_1)(1 - \frac{G_2}{G_1})V_2}{7 - 5v_1 + 2(4 - 5v_1)\frac{G_2}{G_1}} \tag{10}$$

in which $v_1$ is the Poisson's ratio of phase 1, and phase 1 and phase 2 represent the matrix material and the inclusion material respectively.

Using the correspondence principle again and assuming there is no relaxation in Poisson's ratio, Equation(10) becomes

$$G_c^* = G_1^* - \frac{15(1-v_1)(G_1^* - G_2^*)V_2}{7 - 5v_1 + 2(4 - 5v_1)\frac{G_2^*}{G_1^*}} \tag{11}$$

for the complex shear modulus of the composite material. The loss tangent again is complicated to write explicitly, so it is graphically displayed using computed numerical values.

## Platelet inclusions

For a dilute suspension of platelet elastic inclusions of phase 2 in a matrix of phase 1, the shear modulus of the composite $G_c$ was given as(Christensen, 1979)

$$G_c = G_1 + \frac{V_2(G_2-G_1)}{15}\left[\frac{9K_2+4(G_1+2G_2)}{K_2 + \frac{4}{3}G_2} + 6\frac{G_1}{G_2}\right] \tag{12}$$

Again, using the correspondence principle, Equation(12) becomes

$$G_c^* = G_1^* + \frac{V_2 (G_2^* - G_1^*)}{15} \left[ \frac{9K_2^* + 4(G_1^* + 2G_2^*)}{K_2^* + \frac{4}{3}G_2^*} + 6\frac{G_1^*}{G_2^*} \right] \quad (13)$$

for the complex shear modulus of the composite materials.

As for procedure, we remark that although Equations (5) to (13) were developed for the shear modulus of the composite, the shear moduli $G^*$ were replaced by the Young's moduli $E^*$ in the figures for comparison with Fig. 1. The Voigt and Reuss relations given by Equations (1) and (3) apply to $G^*$ as well as to $E^*$. The actual relationship between $E^*$ and $G^*$ and the properties of the constituents of a composite is simple only for certain phase geometries. For example, for some common phase geometries, a Poisson's ratio of 0.3 for each phase gives a Poisson's ratio close to or equal to 0.3 for the composite. However for some phase geometries, a constituent Poisson's ratio of 0.3 can give rise to a negative Poisson's ratio in cellular solids with one phase void (Lakes, 1987) or in unusual laminates (Milton, in press). The calculations are on the basis that $V_1 + V_2 = 1$ except that $V_1 + V_2 = 0.8$ for the multi-phase Hashin elastic bound, for which 20% void by volume fraction is assumed to be contained as a third phase in the composite.

## RESULTS AND DISCUSSION

Results are plotted as stiffness-loss maps (plots of $|E^*|$ vs tan$\delta$) as shown in Figures 2-4.

Figure 2 shows predicted properties of composites containing phases which differ greatly in properties. Steel is considered as phase 1, with $|E_1^*| = 200$ GPa, tan$\delta_1 = 0.001$ and and a viscoelastic elastomer as phase 2, with $|E_2^*| = 0.020$ GPa, tan$\delta_2 = 1.0$. The graph was enlarged in the vicinity of 100% phase 1 and shown in Figure 3 for clarity. A small volume fraction of phase 2 results in a large increase in loss with little reduction in stiffness so that the Reuss structure permits higher losses than the Voigt structure. However, in the Reuss structure each phase carries the full stress, so that a composite of this type will not be strong if, as is usual, the soft phase 2 is weak.

As for 'bounds' on the properties, the curves for the Voigt and Reuss composites enclose a region in the stiffness-loss map, as do the curves for the upper and lower Hashin-Shtrickman composites. It is tempting to think of these curves as 'bounds' on the viscoelastic behavior, however such a surmise has not been proven. They represent extremes of composites which can be fabricated, however we do not yet know if they represent true bounds. Roscoe (1969) has mathematically established bounds for the real and imaginary parts $E'$ and $E''$ of the complex modulus of composites and has shown them to be equivalent to the Voigt and Reuss relations. Therefore the stiffness, expressed

as $|E^*|$ of the composite is bounded from above by the Voigt limit and cannot exceed the stiffness of the stiff phase. This is not quite the same as establishing bounds for a stiffness-loss map since it is not obvious whether a maximum in $\tan\delta = E''/E'$ could be obtained simultaneously with a maximum in $E'$ . In particular, we can construct $\tan \delta_c = E''_{voigt}/E'_{reuss} > E''_{reuss}/E'_{reuss}$ and be within the bounds of Roscoe. We do not yet know if such a composite is physically realizable.

In the stiffness-loss map, the lower and upper two-phase Hashin composites behave similarly to the Voigt and Reuss composites, respectively. This is in contrast to the usual plots of elastic stiffness vs volume fraction, in which the Hashin bounds can differ greatly from the Voigt/Reuss ones. As for the physical attainment of the the Voigt and Reuss composites, simple laminates can be made as in Fig. 1, but these are anisotropic. Isotropic composites which attain the Voigt or Reuss moduli are not considered to be attainable. Isotropic polycrystals attaining the Voigt or Reuss bounds for the bulk modulus are also possible (Avellaneda and Milton, 1989) at the expense of some added structural complexity.

For the three-phase Hashin structure with 20% void content in the composite, the lower curve reduces to zero and is not shown in the graph; the upper bound lies close to the Voigt curve with 20% to 40% lower stiffness as shown in Fig. 2.

The composite containing soft spherical inclusions is also found to behave similarly to the Voigt composite in that a small volume fraction of soft, viscoelastic material has a minimal effect on the loss tangent, though it does reduce the stiffness. As for the composite containing soft platelet inclusions, it is found that the results are similar to those of the Reuss structure. A small volume fraction of platelet inclusions as phase 2 results in a very large increase in loss tangent without any significant reduction in the stiffness. However, soft platelets resemble penny-shaped cracks in the matrix, so that such a composite would be weaker than the matrix, particularly if the matrix were brittle.

Figure 4 shows predicted properties of composites containing phases which do not differ so much in properties as steel and viscoelastic elastomers. Copper as phase 1, with $|E_1^*|$=117 GPa, $\tan\delta_1$= 0.002 and indium as phase 2, with $|E_2^*|$=10.8 GPa, $\tan\delta_2$=0.025 (at 1 kHz) were used for this investigation. Observe that the *shape* of this stiffness-loss map differs from the case of the polymer-metal composite. The implication of this difference in shape is as follows. If the constituents differ by orders of magnitude in stiffness and loss, then the Reuss and platelet composites are orders of magnitude superior to the Voigt and spherical inclusion composites in achieving high stiffness and high loss. If the constituents do not differ so much in their properties,

their composites of various structures do not differ as much either. Composites containing a stiff, low loss material (such as a metal) and a small amount of compliant, high loss material can exhibit a stiffness close to that of the metal, as well as high loss superior to that of a metal-metal composite.

An interesting aspect of the Reuss and platelet composites which give the highest loss (for given stiffness) is that they exhibit highly nonuniform strain fields. The strain in the soft, lossy phase is much larger than the strain in the stiff phase. This is in contrast to the Voigt composite in which the strain in each phase is the same. The re-entrant foams (Chen and Lakes, 1989, in press) with a negative Poisson's ratio also exhibit non-affine deformation of a more complex nature in that the foam cells unfold as the foam is deformed.

# CONCLUSIONS

1. In a stiffness-loss map, the upper and lower two-phase Hashin composites behave similarly to the Voigt and Reuss composites, respectively.
2. Reuss laminates and platelet filled materials based on a stiff, low loss phase and a compliant high loss phase were found to exhibit high stiffness combined with high loss tangent. However, in the Reuss structure each phase carries the full stress, so that a composite of this type will not be strong if, as is usual, the compliant phase is weak.
3. A composite containing soft lossy spherical inclusions in a stiff matrix behaves similarly to the Voigt composite: low loss and a reduction in stiffness.
4. Composites containing a metal and a small amount of compliant, high loss polymer can in principle exhibit a stiffness close to that of the metal, as well as high loss.

# ACKNOWLEDGMENT

# REFERENCES

Ahmed, S., and Jones, F.R. (1990), "A review of particulate reinforcement theories for polymer composites", *J. Materials Sci.*, **25** , 4933-4942.

Avellaneda, M. and Milton, G., (1989) "Optimal bounds on the effective bulk modulus of polycrystals", SIAM J. Appl. Math. **49**, 824-837.

Chen, C.P. and Lakes, R.S., (1991) "Holographic study of conventional and negative Poisson's ratio metallic foams: elasticity, yield, and micro-deformation", J. Materials Science **26**, 5397-5402.

Chen, C.P. and Lakes, R.S., (1989)"Dynamic wave dispersion and loss properties of conventional and negative Poisson's ratio polymeric cellular materials", *Cellular polymers*, **8** , 343-359.

Christensen, R.M., *Theory of viscoelasticity*, 2nd ed., Academic Press, New York, 1982.

Christensen, R.M., *Mechanics of composite materials* , John Wiley & Sons, New York, 1979.

Ferry, J. D. *Viscoelastic properties of Polymers*, 2nd ed J. Wiley, N.Y., 1979

Hashin, Z., (1962) "The elastic moduli of heterogeneous materials", *J. Appl. Mech., Trans.* ASME, **84E**,143-150.

Hashin Z., and B. W. Rosen, (1964),"The elastic moduli of fiber-reinforced materials", *J. Appl. Mech., Trans.* ASME, **31**, 223-232.

Hashin, Z., (1965a),"On elastic behaviour of fibre reinforced materials of arbitrary transverse phase geometry", *J. Mech. Phys. solids*, **13**, 119-134.

Hashin, Z., (1965b), "Viscoelastic behavior of heterogeneous media", *J. Appl. Mech., Trans.* ASME, **32E**, 630-636.

Hashin, Z., (1966), "Viscoelastic fiber reinforced materials", *AIAA Jnl.*, **4**, 1411-1417.

Hashin, Z., (1970), "Complex moduli of viscoelastic composites: I. General theory and application to participate composites", *Int. J. Solids, Structures*, 6, 539-552.

Hashin Z., and Shtrickman, S. (1963),"A variational approach to the theory of the elastic behavior of multiphase materials", *J. Mech. Phys. solids*, **11**, 127-140.

Katz, J. L. (1971),"Hard tissue as a composite material - I. Bounds on the elastic behavior", *J. Biomechanics*, **4**, 455-473.

Lakes, R.S. (1987),"Foam structures with a negative Poisson's ratio", *Science*, **235**, 1038-1040 .

Lakes, R.S. (1991), "Deformation mechanisms of negative Poisson's ratio materials: structural aspects", *J. Materials Science*, **26**, 2287-2292.

Lakes, R.S., Katz, J.L., and Sternstein, S.S., (1979), "Viscoelastic properties of wet cortical bone: Part I, torsional and biaxial studies." *Journal of Biomechanics*, **12**, 657-678.

Milton, G., (in press) "Laminates with a negative Poisson's ratio".

Nielsen, I., *Mechanical Properties of Polymers*, Reinhold, 1962.

Nowick A. S. and Berry, B. S.*Anelastic relaxation in crystalline solids*, Academic, N.Y., 1972.

Roscoe, R, (1969), "Bounds for the real and imaginary parts of the dynamic moduli of composite viscoelastic systems", *J. Mech. Phys. Solids*, **17**, 17-22.

Shipkowitz, A.T., Chen, C.P. and Lakes, R.S., (1988), "Characterization of high-loss viscoelastic elastomers", *Journal of Materials Science*, **23**, 3660-3665.

Zener, C. *Elasticity and anelasticity of metals*, University of Chicago Press, 1948.

Fig. 1

(a)            (b)            (c)

Fig. 2
Chen, lakes

Fig-3
(bottom...)

Fig. 5
Brinkman

May 1, 1992

Professor Roderic Lakes
College of Engineering
The University of Iowa
Iowa City, Iowa 52242

Dear Professor Lakes:

    I would like to invite you to give a technical seminar on foams to the DuPont Composites Division in Wilmington, Delaware at a mutually convenient time. We would be prepared to cover your travel expenses. I look forward to hearing from you.

Sincerely,

*Dennis A. Nollen*
Dennis A. Nollen, Ph.D.
Research Associate
(302) 999-2901

*Talk 18 May 92*
*Possibly*
*mid June.*

DAN:bam

# Journal of Materials Science

# Holographic study of conventional and negative Poisson's ratio metallic foams: elasticity, yield and micro-deformation

C. P. CHEN, R. S. LAKES*
*Department of Mechanical Engineering, and * also Department of Biomedical Engineering, and Center for Laser Science and Engineering, University of Iowa, Iowa City, IA 52242, USA*

An experimental study by holographic interferometry is reported of the following material properties of conventional and negative Poisson's ratio copper foams: Young's moduli, Poisson's ratios, yield strengths and characteristic lengths associated with inhomogeneous deformation. The Young's modulus and yield strength of the conventional copper foam were comparable to those predicted by microstructural modelling on the basis of cellular rib bending. The re-entrant copper foam exhibited a negative Poisson's ratio, as indicated by the elliptical contour fringes on the specimen surface in the bending tests. Inhomogeneous, non-affine deformation was observed holographically in both foam materials.

## 1. Introduction

Conventional foams, like other ordinary materials, exhibit a positive Poisson's ratio, that is, they become smaller in cross-section when stretched and larger when compressed. Recently, the invention of negative Poisson's ratio foams was reported [1-3]. Foam materials based on metal and several polymers were transformed so that their cellular architecture became re-entrant, i.e. with inwardly protruding cell ribs. Foams with re-entrant structures exhibited negative Poisson's ratios as small as − 0.7, as well as greater resilience, than conventional foams.

Material properties of conventional and re-entrant copper foams have been determined from uniaxial compression tests using an MTS materials testing machine [3]. Engineering stress–strain graphs were extracted from load–displacement data. The Poisson's ratios of specimens in this series were determined from displacement measurements of high magnification video tapes of the tensile tests. However, other methods, which complied with ASTM standards, of measuring Poisson's ratio were tried and found unsuitable due to the inherently rough, porous surface of the foams.

The laser interferometric method has been presented in the literature for determining the displacement field on the surface of a specimen and therefore the specimen's properties. The hyperbolic contour lines on the lateral surface of a bent specimen can be viewed interferometrically and used to determine the specimen's Poisson's ratio [4]. The deformation of an object can be investigated from the fringes on a holo- gram film by means of double-exposure holographic interferometry [5]. It has also been concluded that the laser interferometry technique offered a very useful and reliable tool to determine the Poisson's ratio of orthotropic fibre reinforced plastics (FRP) plates [6].

Holographic interferometry provides interferometric accuracy for deformation measurements of rough surfaces; this feature is of particular use for cellular solids.

For deformation mechanisms and structure-related behaviour, rotational degrees of freedom were examined in earlier articles [7, 8]. The method involved inference from non-classical size effects in the bending and torsion rigidity as determined using a micro- mechanics apparatus. Moreover, dispersion of stand- ing waves and cut-off frequencies in torsional vibration were observed for the foam materials [9]. These non-classical phenomena were attributed to the material microstructure in a structural view.

The present study applies double-exposure holo- graphic interferometry to determine the material properties (Young's moduli, Poisson's ratios, and yield behaviour) of conventional and negative Poisson's ratio foam, as well as to explore the non- affine deformation associated with movements of the microstructure. Affine deformation is locally equi- valent to a superposition of a strain and a rotation.

## 2. Materials and methods

Bending experiments were conducted upon conven- tional and re-entrant copper foam specimens at room temperature. The conventional copper foam used was open cell with density 0.795 g cm$^{-3}$, solid volume frac- tion 0.089, and cell size 0.4 mm. The copper foam was transformed into re-entrant structure by successive applications of small increments of plastic deforma- tion in three orthogonal directions, as desribed earlier [1, 3]. The density of the re-entrant copper foam tested here was 2.43 g cm$^{-3}$ with a permanent volu- metric compression ratio of approximately 3, and solid volume fraction 0.27. The foams were machine finished to obtain the desired surface smoothness. The

dimensions of the conventional copper foam specimen were 9 mm by 15 mm in cross-section and 34 mm in length; and of the re-entrant specimen, 6 mm by 6.5 mm in cross section and 26 mm in length.

The lower end of each specimen was cemented firmly on a precision tilt/rotation base. The upper specimen end was cemented to an aluminium cantilever beam upon which weights were placed to achieve bending. The aluminium beam was sufficiently long for it to be possible to neglect the axial compression caused by the weight in comparison with strain due to bending. The specimen was thus deformed by a nearly pure bending moment. The fringe pattern was centred to facilitate the determination of Poisson's ratio from the hyperbolic or elliptical fringe pattern. This was done by tilting and rotating the base between the holographic exposures.

The specimens and the holographic components were installed on a research-grade damped table top supported upon four pneumatic isolation mounts. The laboratory ventilation was shut off during the experiments to eliminate air currents and noise. A beam from a 15 mW helium–neon laser was divided by a beamsplitter into an object beam and a reference beam. The following configuration was used for zero-order fringe analysis described below. Image plane transmission holograms were made of the tensile side of the bent specimen via a unity magnification configuration using a six-element coated $f/1.2$ lens system of focal length 150 mm. For the purpose of simplifying the calculation, the reference and reconstruction beams were collimated. Moreover the object illumination beam was collimated and directed perpendicular to the specimen surface by a plate beamsplitter, as shown in Fig. 1. Each exposure was about 3 s, achieved using a digitally controlled shutter. Further image plane holograms were made, without specimen tilt, for Haidinger fringe analysis using an $f/0.7$ lens system consisting of two $f/1.4$ camera lenses of 50 mm focal length and seven elements each, placed front to

front. The rationale was to improve the quality of the Haidinger fringes and achieve a wider exit cone of projected rays. Agfa 8E75 holographic film was used, was developed in Kodak D19 and bleached in ammonium dichromate bleach to increase the brightness. The images were viewed in laser light of 633 nm wavelength, the same as was used for making the holograms.

## 2.1. Bending test: zero-order fringe interpretation

The zero-order fringe method (ZF) [5] was used to obtain the specimen's Young's modulus and Poisson's ratio, for study of residual strain due to yielding, and for study of inhomogeneous deformation. The relation between the displacement vector, $u$, and the fringe order, $n$, at a point, $P$, on the illuminated surface of the specimen is given by

$$n\lambda = u \cdot (k - h) \qquad (1)$$

in which $\lambda$ is the wavelength of the light, $k$ is the unit vector from the object to the observer's eye, and $h$ is the unit vector from the light source to the object. The fringe order $n$ represents the total displacement vector of points on the specimen surface. The centre of the fringe pattern was the location where the lateral movement was zero.

Equation 1 is simplified if the illumination and observation directions are arranged to be collinear in the $z$-direction perpendicular to the specimen surface. This was achieved in the experiment via the configuration shown in Fig. 1. Collimated object illumination was used so that the illumination direction did not vary with position. Under these conditions, Equation 1 becomes

$$\frac{n\lambda}{2} = u_z \qquad (2)$$

in which $u_z$ is the displacement of point $P$ in the $z$-direction (out-of-plane, along the line of sight) and can be obtained from the fringe order $n$.

The macroscopic strain, $\varepsilon$, on the lateral surface of the beam as a result of bending deformation was given as [10]

$$\varepsilon = \frac{2y}{L^2} u_z \qquad (3)$$

in which $y$ is the distance from the point, $P$, at which the strain is measured to the neutral surface of the beam or one-half of the beam thickness for a rectangular cross-section specimen, and $L$ is the distance between point $P$ and the centre of the fringe pattern. The Young's modulus, $E$, of the specimen is defined as $E = \sigma/\varepsilon$, or, from the elementary theory of bending in classical elasticity

$$E = \frac{ML^2}{2u_z I} \qquad (4)$$

in which $M$ is the bending moment, and $I$ is the moment of inertia of the cross-sectional area of the specimen.
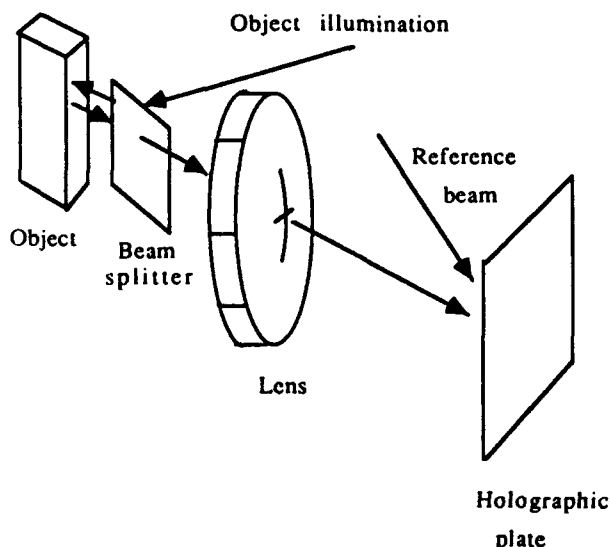


Figure 1 Configuration for image plane holography with collimated illumination along the optic axis.

The fringe pattern on the specimen's surface can also be used for determining the specimen's Poisson's ratio, $v$. The contour lines of constant $u_z$ were given, based on classical elasticity, as [4]

$$z^2 - vy^2 = \text{constant} \qquad (5)$$

The contour lines of the lateral displacement field of the specimen, or the observed interference fringes, are therefore hyperbolae for specimens of positive Poisson's ratio and ellipses for those of negative Poisson's ratio, respectively. The Poisson's ratio, $v$, was also given as

$$v = \tan^2\alpha \qquad (6)$$

in which $2\alpha$ is the angle between the asymptotes of the hyperbolae as given by Equation 5.

Holographic exposures were made of bent specimens at progressively larger loads, with the aim of exploring the onset of inhomogeneous deformation associated with the microstructure as manifested by irregularity and breakup of the fringe pattern.

This holographic interferometry and data reduction scheme was first verified by tests upon a PMMA (polymethyl methacrylate or Plexiglas®) specimen, which has independently determined properties [11]. The PMMA specimen was 9 mm by 12.5 mm in cross-section and 88 mm in length. White paint was sprayed on the illuminated surface of the PMMA specimen for the purpose of maximizing the diffuse light reflection.

## 2.2. Yielding test

A holographic exposure was made of the specimen without any bending load. The bending load was then applied for 30 s and removed. The second exposure was taken 30 s later after the load was removed. If yielding has occurred, there will be some residual strain, resulting in fringes in the hologram. Based on a series of holograms taken with increasing loads, the yield strength of the specimen was determined.

## 2.3. Study of non-affine deformation

Non-affine deformation was studied both by the zero-order fringe method and by the Haidinger fringe method. In the zero-order fringe method, in-homogeneous deformation of the non-affine type manifests itself as a bumpiness or breakup of the fringes covering the specimen. The optical system in Fig. 1, used for zero-order fringe analysis, is sensitive to out-of-plane deformation, perpendicular to the specimen surface, so that is also the sensitivity direction for non-affine deformation. The Haidinger fringe method discloses the vector displacement of an individual object point [5, 12]. The $x$ component of in-plane displacement, $U_x$, is given by

$$U_x = \lambda/\xi_x \qquad (7)$$

in which $\lambda$ is the wavelength of light and $\xi_x$ is the $x$ component of angular spacing, in radians, of the projected fringes; similarly for the $y$-direction. In this method, the corresponding image point was illuminated by a concentrated laser beam, focused to a spot
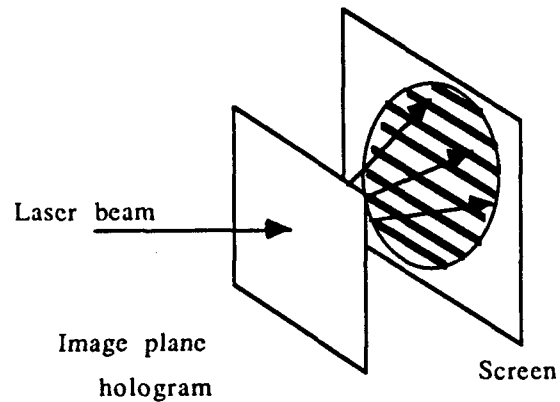


Figure 2 Projection of fringes from an image point in the Haidinger fringe method.

size less than 0.2 mm diameter, in the direction of the original reference beam. Diffracted light formed a pattern of fringes which was projected upon a ground glass, as shown in Fig. 2. The light beam was slowly scanned across the specimen and inferred displacements of nearby points were compared to determine the micro-strain. In this experiment, non-affine deformation manifests itself as micro-strain differing from macroscopic strain.

## 3. Microstructural analysis

The mechanical properties of foams can be related to the properties of the cell material and geometry [13]. For conventional open cell foam [13]

$$\frac{E}{E_s} = \left(\frac{\rho}{\rho_s}\right)^2 \qquad (8)$$

on the basis of simple bending of the cell ribs, in which $E$ and $\rho$ are the Young's modulus and mass density of the foam, and $E_s$ and $\rho_s$ are the Young's modulus and mass density of the solid of which the foam was made.

Cellular materials can collapse. Plastic collapse occurs when the moment exerted on the cell ribs exceeds the fully plastic moment, creating plastic hinges. The plastic collapse stress, or the yielding strength of the foams was given as [13]

$$\frac{\sigma_y}{\sigma_{ys}} = 0.3\left(\frac{\rho}{\rho_s}\right)^{3/2} \qquad (9)$$

in which $\sigma_y$ and $\sigma_{ys}$ are the yield strength of the foam, and the solid of which the foam was made, respectively.

The properties of solid copper were taken as $E_s = 119\,000$ MPa, $\rho_s = 8.93$ g cm$^{-3}$, and $\sigma_{ys} = 62$ MPa [13, 14]. Substitution of the foam densities mentioned in the previous section in Equations 8 and 9 yielded theoretical values of the foam properties. The Young's modulus, $E$, and yield strength, $\sigma_y$, of the conventional copper foam were predicted to be 943 and 0.49 MPa, respectively. The prediction of the properties of the re-entrant foams was not attempted because Equations 8 and 9 are only applicable to conventional foams with straight cell ribs.
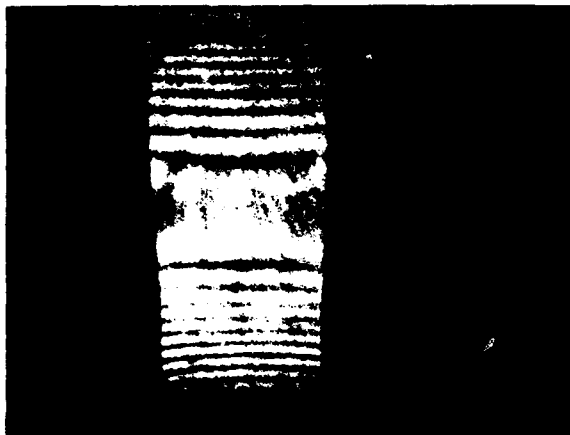
*Figure 3* Fringe pattern of PMMA by holographic interferometry, bending test.



*Figure 5* Yielding of (■) conventional and (▲) re-entrant foam in bending. Residual strain versus applied strain, both in units of microstrain.

## 4. Results and discussion

A typical fringe pattern of the PMMA specimen is shown in Fig. 3. Analysis of the fringe orders at different locations via Equation 3 disclosed that uniform strain was obtained on the specimen surface in bending. The Young's modulus, $E$, was obtained to be approximately 2.6 GPa, and the Poisson's ratio, $v$, was obtained to be 0.33 from Equations 4, and 6, respectively. The experimental values of $E$ and $v$ were in good agreement with those independently determined [11]. The fringes of the hyperbolic contour lines remained of high contrast up to high fringe density corresponding to a bending strain 0.000 84. Consequently, the PMMA did not exhibit any inhomogeneous deformation, as expected in view of classical elasticity or viscoelasticity.

Fig. 4 shows the fringe pattern of the conventional copper foam. These fringes represent hyperbolic contour lines which show the anticlastic curvature of a positive Poisson's ratio material, just as the case with PMMA. The measured asymptotic angle, $\alpha$, was substituted into Equation 6 to obtain the Poisson's ratio, $v$, of the conventional copper foam as 0.25. Conventional foams usually have Poisson's ratios
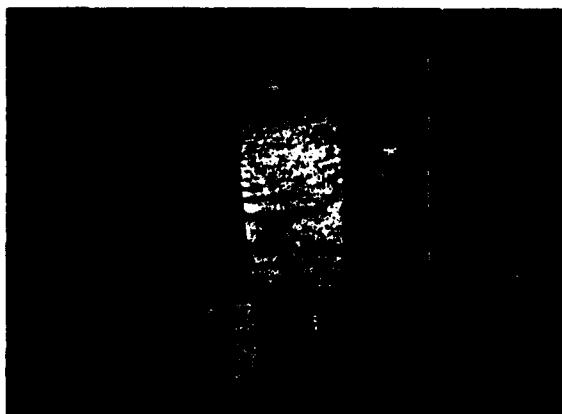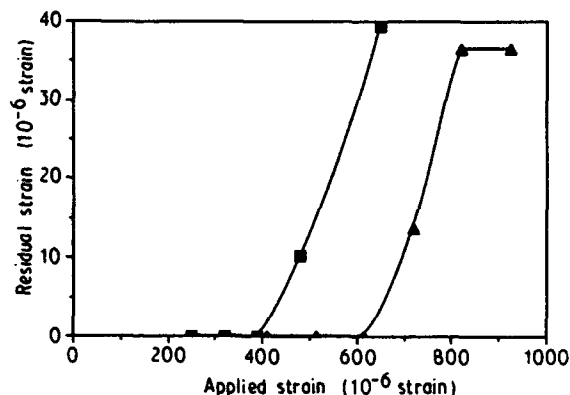
closer to 0.3, but there is considerable variation [13]; indeed, a different density copper foam [3] had a Poisson's ratio of 0.4. The Young's modulus, $E$, was found to be approximately 900 MPa, at a macroscopic stress 0.15 MPa and strain 0.000 17. The experimental value of $E$ agreed reasonably well with 943 MPa predicted from Equation 8 in the previous section. Fig. 5 shows the residual strain plotted versus the applied strain for conventional copper foam obtained by the yielding tests. The yield strength, $\sigma_y$, of the conventional copper foam was found to be approximately 0.42 MPa. The yield strength predicted by Equation 9 was 0.49 MPa. The agreement is considered satisfactory in view of the fact that a book value for the 0.2% yield strength of solid copper was used in the calculation. The yield strain of the foam was 0.000 47.

The fringe pattern for the foams became less clear as the load level increased. On close examination, the fringes were seen to become progressively more bumpy with increase in load. The clarity of the fringe pattern was represented quantitatively by $d/D$, in which $d$ is the width of the pattern of bumps of two neighbouring fringes and $D$ is the overall fringe width, and is shown in Fig. 6, with an estimated 10% error



*Figure 4* Fringe pattern of conventional copper foam in bending by holographic interferometry, density 0.795 g cm⁻³ with solid volume fraction 0.089.
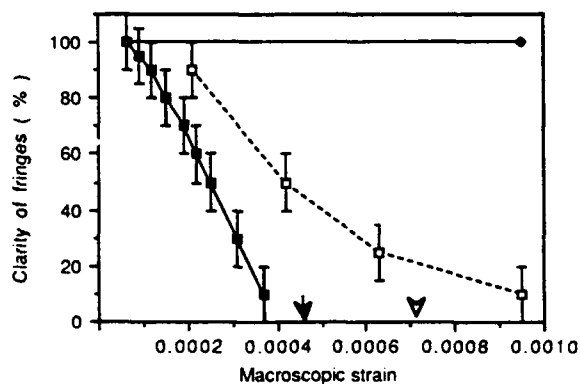


*Figure 6* The clarity of the fringe pattern versus the macroscopic strain, $\varepsilon$, bending test. (- ■ —) Conventional copper foam, (▼) the yield point. (-- ◻ --) Re-entrant copper foam, (▽) the yield point. (◇) PMMA.
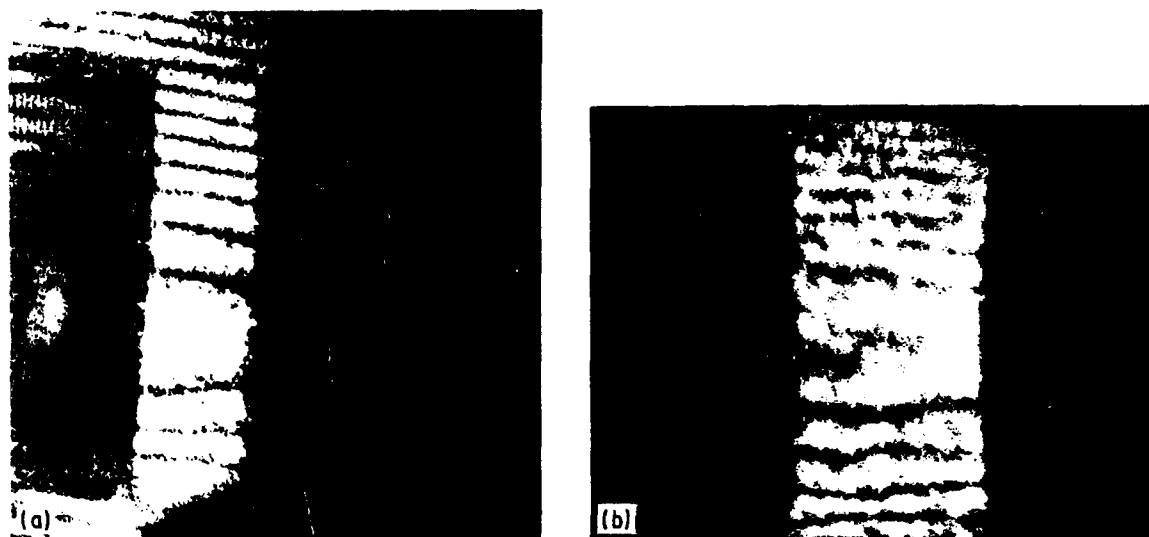
*Figure 7* Fringe pattern of negative Poisson's ratio copper foam in bending by holographic interferometry, density 2.43 g cm$^{-3}$ with solid volume fraction 0.27. (a) Lower load, (b) higher load.

range. As progressively higher loads were applied to conventional foam, fringes began to become bumpy at strains of 0.000 062 and were very broken up at strains of $\varepsilon = 0.000\,32 - 0.000\,37$. Complete fringe breakup occurred at strains below the yield strain and so cannot be a result of yielding.

Fig. 7 shows the fringe pattern of the re-entrant copper foam. The fringe pattern of elliptical contour lines indicated that the Poisson's ratio of the re-entrant copper foam was negative. The Young's modulus, $E$, was obtained to be approximately 480 MPa, at a macroscopic stress of 0.032 MPa and strain 0.000 67. This result is consistent with the fact that the Young's modulus of the foam materials has previously been found to be reduced by re-entrant transformation [3]. The Poisson's ratio, $v$, for this specimen was obtained to be $-0.11$; lower density copper foam [3] in simple compression had a Poisson's ratio of $-0.4$. Fig. 6 shows the residual strain as it depends on the applied strain of the re-entrant copper foam. The yield strength was determined to be 0.35 MPa by the yielding tests, and the yield strain was 0.000 72.

The predictions of the properties of the conventional copper foams by Equations 8 and 9 on the basis of solid volume fraction were obtained with some structural assumptions. However, the yield strength, $\sigma_y$, of the foam materials can also be obtained by substituting Equation 8 into Equation 9 to obtain $\sigma_y/\sigma_{ys} = 0.3(E/E_s)^{3/4}$ with the solid volume fraction eliminated. With $E = 480$ MPa substituted, the yield strength $\sigma_y$ for re-entrant copper foam was calculated from this expression to be 0.3 MPa. This was comparable to 0.35 MPa obtained by the yielding tests on the re-entrant copper foam even though Equations 8 and 9 individually do not apply to re-entrant foam.

Fringes in the re-entrant foam began to get bumpy at a macroscopic strain of 0.000 21 and were totally broken up at a strain of from 0.000 63-0.001. In this

case the strain for total fringe breakup and the strain for yield were comparable. Nevertheless, the onset of fringe bumpiness or breakup occurred well below the yield point, as shown in Fig. 6.

The loss of fringe clarity in the foams at higher loads was not a single loss of contrast associated with a hologram of a field of homogeneous strain and rotation [5] viewed through a large pupil; there was no such effect in the PMMA which is a homogeneous material. The fringes in the foam became noticeably bumpy before they broke up. The effect is attributed to inhomogeneous deformation associated with the microstructure, specifically a non-affine deformation which cannot be described as a superposition of homogeneous strain and rotation. Quantitative measures of such inhomogeneous deformation may be defined as follows: the ratio $\Gamma$ of micro-strain to macro-strain $\varepsilon_{macro}$, $\Gamma = (\delta/d_{cell})/\varepsilon_{macro}$; and a micro-deformation characteristic length $l_m = \delta/\varepsilon_{macro}$ in which $\delta$ is the inhomogeneous micro-deformation and $d_{cell}$ is the cell size. In the present zero-order fringe experiments the fringes become totally fragmented when the micro-deformation over one cell is one fringe or half a wavelength of red light, so $\delta = 0.3$ μm. The cell size is 0.4 mm for conventional foam and $0.4\,\text{mm}/(3)^{1/3}$ for re-entrant foam. Consequently, for conventional foam, $\Gamma_{avg, \perp} = 2.1$, $l_m = 0.86$ mm; for re-entrant foam, $\Gamma_{avg, \perp} = 1.3$, $l_m = 0.38$ mm. The non-affine motion disclosed by these experiments is an average value perpendicular to the specimen surface.

The Haidinger fringe experiments disclosed largely in-plane motions along the specimen long axis. The calculated micro-strains ranged from $-0.004$ to $0.004$ for a macro-strain of 0.000 79, for the conventional copper foam; and from $-0.0013$ to $0.0028$ at a macro-strain of 0.0008 for the re-entrant copper foam. The ratios of the maximum micro-strain to the macro-strain were thus determined to be $\Gamma_{max, \parallel} = 5.1$, and 3.5 for the conventional copper foam, and the re-entrant

copper foam, respectively. The non-affine motion disclosed by these experiments is a maximum value parallel to the specimen surface.

The inhomogeneous, non-affine micro-deformation observed in the foams has several interesting implications. For example, such deformation, as well as a local rotation of points has been incorporated into generalized continuum theories known as "microstructure" [15] or "micromorphic" [16] elasticity. In comparison, Cosserat solids [7, 8] admit rotations and translations, and classically elastic solids admit only translation of points. A material obeying generalized continuum theory may exhibit stress concentration factors which are less or greater than classical values, depending on the values of the extra material constants prescribed by the theory [17]. The micro-deformation and local rotation degrees of freedom are therefore intimately connected with the toughness of these materials. The micro-deformation is, moreover, associated with unusual acoustic behaviour, both in the context of generalized continuum mechanics [15], and experimental dynamic measurements [9]. However, we do not at this time have the ability to predict or control the acoustic behaviour based on non-affine deformation kinematics. Microstructural degrees of freedom are also associated with the Poisson's ratio: negative Poisson's ratios may result from non-affine deformation kinematics or from rotational degrees of freedom combined with prestrain [18]. Rotational freedom is doubtless present in view of the bending moments transmitted through the cell ribs [2]; however, that alone need not give rise to a negative Poisson's ratio [18]. The present study has demonstrated the presence of non-affine deformation in both the conventional and re-entrant metal cellular solids. We remark that the measurements were made at the specimen surface, where some cells were incomplete as a result of cutting. Consequently, there is the possibility that the surface is not equivalent to the bulk material. The larger non-affine effects in the conventional foam were surprising in view of qualitative observations of unfolding of cells in stretched re-entrant polymer foam, which suggested that larger effects would occur in the re-entrant material. However, it cannot be assumed that the deformation kinematics are identical in the polymeric and metallic foams; further study is anticipated to resolve this issue.

## 5. Conclusions

1. The holographic interferometry technique was found to be a useful method to determine the elastic properties of the foam materials. It was verified by using it to examine a PMMA specimen, which has independently determined properties.

2. The Young's modulus, $E$, yield strength, $\sigma_y$, and Poisson's ratio, $v$, of the conventional and negative Poisson's ratio copper foams were determined in bending tests by the holographic interferometry. The Young's modulus of the conventional copper foam was found to be twice that of the corresponding re-entrant negative Poisson's ratio foam. The yield strength was approximately the same for the conventional and negative Poisson's ratio copper foams.

3. The Young's modulus and yield strength of the conventional copper foam were comparable to those predicted by microstructural analysis based on cellular rib bending.

4. Inhomogeneous, non-affine deformation was inferred from the bumpiness and breakup of the holographic fringes with increasing load. The effects were larger in the conventional foam.

## References
1. R. S. LAKES, Science 235 (1987) 1038.
2. Idem, ibid. 238 (1987) 551.
3. E. A. FRIIS, R. S. LAKES and J. B. PARK, J. Mater. Sci. 23 (1988) 4406.
4. S. P. TIMOSHENKO and J. N. GOODIER, "Theory of elasticity", 3rd Edn (McGraw-Hill, New York, 1970).
5. W. SCHUMANN and M. DUBAS, "Holographic interferometry" (Springer-Verlag, Berlin, 1979).
6. R. M. ,. G. K. RAO, M. SWAMINADHAM and K. RAJANNA. Fibre Sci. Technol. 15 (1981) 235.
7. R. S. LAKES. J. Mater. Sci. 18 (1983) 2572.
8. Idem, Int. J. Solids Struct. 22 (1986) 55.
9. C. P. CHEN and R. S. LAKES. Cell. Polym. 8 (1989) 343.
10. S. P. TIMOSHENKO and J. M. GERE, "Mechanics of materials" (Litton Educational, New York, 1972).
11. J. D. FERRY, "Viscoelastic Properties of Polymers", 2nd Edn (Wiley, New York, 1970).
12. J. BRIERS. Opt. Quant. Electron. 8 (1976) 469.
13. M. F. ASHBY, Metall. Trans. 14A (1983) 1755.
14. C. CARMICHAEL, "Kent's Mechanical Engineers' Handbook", Wiley engineering handbook series, 12th Edn (Wiley, New York, 1950).
15. R. D. MINDLIN, Arch. Rational Mech. Anal. 16 (1964) 51.
16. A. C. FRINGEN, in "IUTAM symposium, Mechanics of Generalized Continua", edited by E. Kröner (Springer-Verlag, Berlin, 1968).
17. J. L. BLEUSTEIN, Int. J. Solids Struct. 2 (1960) 83.
18. R. S. LAKES, J. Mater. Sci. 26 (1991) 2287.

# Journal of Materials Science

# Deformation mechanisms in negative Poisson's ratio materials: structural aspects

R. LAKES
*Departments of Biomedical Engineering, and Mechanical Engineering, and Center for Laser Science and Engineering, University of Iowa, Iowa City, IA 52242, USA*

Poisson's ratio in materials is governed by the following aspects of the microstructure: the presence of rotational degrees of freedom, non-affine deformation kinematics, or anisotropic structure. Several structural models are examined. The non-affine kinematics are seen to be essential for the production of negative Poisson's ratios for isotropic materials containing central force linkages of positive stiffness. Non-central forces combined with pre-load can also give rise to a negative Poisson's ratio in isotropic materials. A chiral microstructure with non-central force interaction or non-affine deformation can also exhibit a negative Poisson's ratio. Toughness and damage resistance in these materials may be affected by the Poisson's ratio itself, as well as by generalized continuum aspects associated with the microstructure.

## 1. Introduction

A new class of cellular materials was reported previously [1]; these materials exhibit a negative Poisson's ratio. Such materials expand laterally when stretched and contract laterally when compressed. This unusual characteristic is achieved by forming the cells into a "re-entrant" shape which bulges inwards and which unfolds under tension resulting in a lateral expansion. These cellular solids can be made from a variety of polymers [1] or from metals [1, 2]. Negative Poisson's ratio materials are of interest because of their unusual nature, and because they deform in ways unexpected on the basis of experience with ordinary materials. For example, their shear modulus can substantially exceed their bulk modulus, a situation opposite that seen in rubbery materials. Moreover, many relationships for deformation in the theory of elasticity contain terms $(1 - v^2)$ with $v$ as Poisson's ratio, so that for $v$ approaching its lower limit $-1$, enhanced shear rigidity or high toughness can be achieved [1], which can be of use in various applications [3]. The materials also exhibit unusual acoustic properties related analytically to the Poisson's ratio [4, 5], as well as acoustic properties experimentally determined and directly related to the re-entrant structure [6].

Negative Poisson's ratios can also arise in two-dimensional honeycombs with inverted cells [7], in rocks with microcracks [8, 9], in an anisotropic microcellular polymer, expanded polytetrafluoroethylene [10, 11], in anisotropic fibrous media in some directions [12-14], in anisotropic pyrolytic carbon [15]. While it had been reported that single-crystal pyrites had a negative Poisson's ratio, recent study indicates otherwise [16]. Thin (anisotropic) magnetized ferromagnetic films have been reported to exhibit a transient negative Poisson's ratio which disappears with ageing [17]. Macroscopic structures of sliders, hinges, and springs can also exhibit negative Poisson's ratio [18]. A variety of structural models can give rise to a negative Poisson's ratio [19], nevertheless negative Poisson's ratios are unusual. Indeed, in a large compilation of properties of polycrystalline materials [20], most have Poisson's ratio in the vicinity of 1/3 with exceptions such as beryllium which has a Poisson's ratio of about 0.1, and ammonium chloride which assumes a negative value over a narrow temperature range.

It is the purpose of this article to identify the relevant microstructural features associated with negative Poisson's ratio materials and to present several structural models which exhibit these features in isolation. In the next section the role of structure in determining Poisson's ratio is explored, and in the section following that, the connection between structures of interest and generalized continuum mechanics is examined.

## 2. Microstructure and Poisson's ratio
### 2.1. Cauchy relations

In the early development of the theory of elasticity, it was believed by some (such as Navier and Poisson) that isotropic materials were describable by only one elastic constant and that Poisson's ratio was 1/4 for all isotropic materials. The basis for this view (so-called uniconstant theory) was an atomic model in which the atoms as point particles in a centrosymmetric lattice [21] interacted by central forces dependent upon distance alone. Based on such a model, the tensorial elastic constants of an anisotropic solid become related by "Cauchy relations"; for an isotropic medium, the Cauchy relations imply a Poisson's ratio of 1/4 for all materials described by the model. These arguments have been recapitulated by modern authors [21-23].
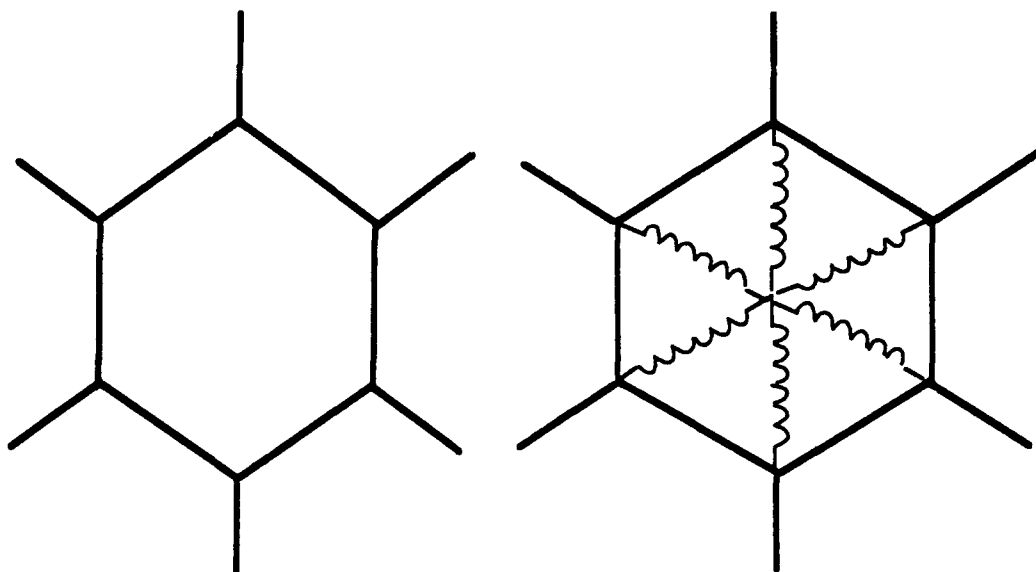
*Figure 1* Hexagonal honeycomb structure of bendable ligaments.

Experiments disclosed Poisson's ratios for most common isotropic materials to be close to 1/3, resulting in the abandonment of uniconstant elasticity theory governed by the Cauchy relations. The classical theory of elasticity now used incorporates two independent elastic constants for isotropic materials, and we realize that the above simple model does not have general applicability.

Poisson's ratios differing from 1/4 can arise from deviations from the above assumptions, specifically (i) non-central forces between particles in the solid, (ii) forces which do not depend on distance alone, or (iii) anisotropy, including noncentrosymmetry. We address in this article the question of what kind of interaction results in a Poisson's ratio which is negative, not just different from 1/4. To that end, we consider several microstructures with the aim of distinguishing which kinds of interaction are most important to achieve a negative Poisson's ratio. Most of these structures are two-dimensional and isotropic in plane in their classical elastic properties either by virtue of the choice of the elastic stiffness of the micro-elements or by symmetry. As for symmetry, materials which are structurally hexagonal, are transversely isotropic, i.e. isotropic in plane, within the framework of classical elasticity [24]. The range for Poisson's ratio, v, for isotropic materials is $-1 < v < 1/2$ in three dimensions and $-1 < v < 1$ in two dimensions.

Under static conditions, noncentral forces must be accompanied by a moment, to satisfy the equilibrium equations. The kinematical variable conjugate to a moment is a rotation angle. As for forces which do not depend on distance but instead connect only selected pairs of particles, the corresponding kinematical deformation is a non-affine one. This is in contrast to affine deformation in which the particles in the solid move in a way corresponding to a uniform strain plus a rotation in a continuum, i.e. $u_j = a_{jk}x_k$ in which $u_j$ is the displacement, $x_k$ is the particle position, $a_{jk}$ is a tensor describing the deformation, and repeated indi-

ces are summed over. Affine deformation kinematics are necessary conditions for the Cauchy relations to be obtained [21].

## 2.2. Non-affine deformation

A honeycomb composed of regular hexagonal cells (Fig. 1) has a Poisson's ratio of $+1$ [7, 25]. The cell ribs undergo bending if the honeycomb is stretched or sheared. The deformation is not affine because some pairs of nodal points move apart during stretching while others do not. Indeed, a honeycomb without any bending can be made of elastic (spring) elements free to rotate at the joints. Because they would rotate without stretching if the honeycomb were under tension, such a structure has a zero Young's modulus. To obtain an elastic honeycomb, additional soft elements could be inserted to supply the restoring force; the Poisson's ratio would be slightly less than 1.

Re-entrant honeycomb cells such as those shown in Fig. 2 give rise to a negative Poisson's ratio [25, 26]. The ligaments undergo bending and the deformation is manifestly non-affine in that the cells unfold during stretching of the honeycomb. In particular, points A and B move further apart than expected from the global strain, while points C and D maintain their separation during stretching. Again, bending is not essential in that a similar effect can be achieved with stretchable (spring) elements only, which are free to pivot with no rotational constraint. The structure is orthotropic, however by appropriate choice of the rib widths and angles, an elastically isotropic honeycomb with a Poisson's ratio of $-1$ can be obtained. For comparison, a structurally hexagonal re-entrant honeycomb structure is shown in Fig. 3; this is isotropic in plane by virtue of symmetry. In this case as well, the bendable ligaments can be replaced by rigid ones which are free to pivot, and the restoring force supplied by elastic elements (not shown).
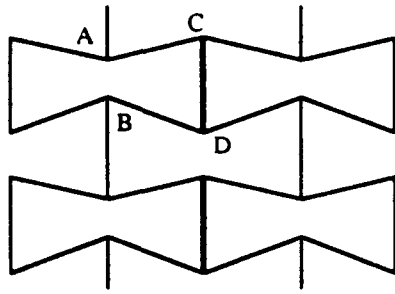
*Figure 2* Re-entrant honeycomb with negative Poisson's ratio, made of bendable ligaments. A similar structure can be made with rigid ligaments if a spring is placed between points of type A and B.
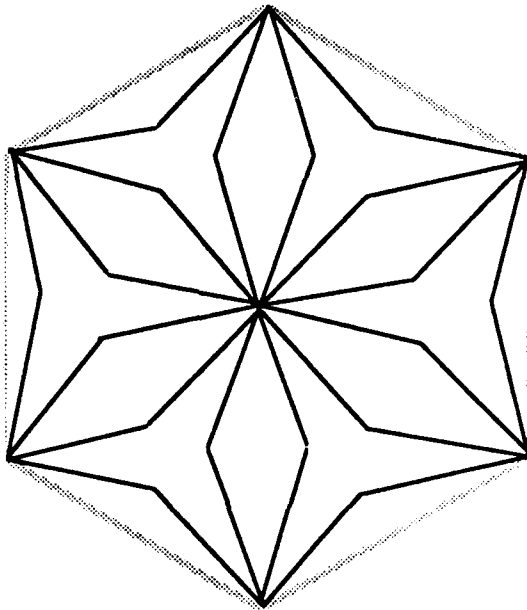


*Figure 4* Lattice of rigid rotatable nodes linked by elastic ligaments.



*Figure 3* Structurally hexagonal re-entrant honeycomb with negative Poisson's ratio. Solid lines are bendable ribs.



*Figure 5* Behaviour of structure shown in Fig. 4. Poisson's ratio versus rotatable node size, $r$, divided by lattice spacing, $d$, and spring stiffness ratio $k_3/k_1$, which is a measure of the relative magnitude of the noncentral forces. Poisson's ratio is positive if all the ligament stiffnesses are positive. ($\square$) $k_3/k_1 = 1$, ($\blacksquare$) $k_3/k_1 = 2$, ($\blacktriangle$) $k_3/k_1 = 5$. ($+$) $k_3/k_1 = 1/2$.

## 2.3. Non-central forces

The above examples indicate it is possible to obtain large magnitudes of Poisson's ratio, including negative values, using central force interactions alone. These structures deform in a non-affine manner. We now consider the effect of non-central forces alone, with affine deformation. A two-dimensional structure of rigid rotatable nodes linked by elastic ligaments, originally examined in a study of generalized continuum mechanics [27], is of interest in this vein and is shown in Fig. 4. The sturcture is cubic, however it is possible to obtain elastic isotropy by choice of the stiffnesses of the elastic ligaments. Given the Lamé and Cosserat elastic constants provided in [27], we invoke isotropy (which results in a relationship between stiffnesses), set up the lattice without prestrain in any of the ligaments, and calculate the engineering elastic constants in terms of the node size and the relative magnitude of the noncentral forces. Calculated Poisson's ratios are shown in Fig. 5. Observe that a rotatable node size of zero or a zero stiffness for the ligaments, $k_3$, which are attached to the rotatable node periphery, results in a lattice governed by purely central forces; the Poisson's
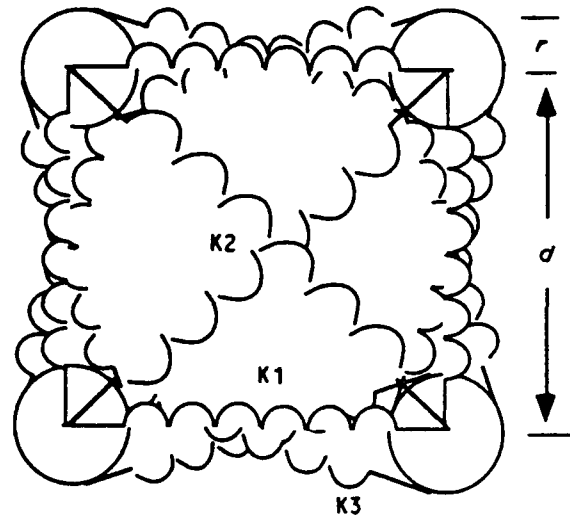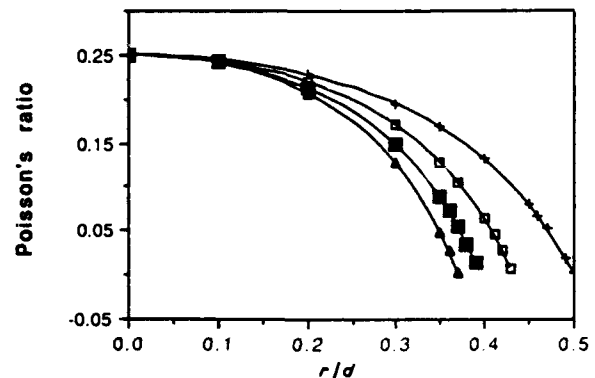
ratio is 1/4 as is the case in three dimensions. Introduction of non-central forces reduces the Poisson's ratio; however, negative Poisson's ratios are not obtained unless one of the ligament stiffnesses becomes negative. Such a ligament would be unstable if isolated, but the stability criterion for the entire lattice remains $-1 < \nu < 1$. If the restriction of isotropy in this structure is relaxed, the minimum Poisson's ratio is still zero for non-negative ligament stiffness. The structure in Fig. 4 may be considered in relation to an earlier analytical study of granular materials [28]. Negative Poisson's ratios are theoretically possible in such granular systems if the stiffness for tangential deformation were to exceed that for normal deformation. However for spherical granules with perfect slip, $\nu = 1/4$, while for contact without slip, $0 \leq \nu \leq 0.11$, consequently Poisson's ratio is positive for real granular materials.

Non-central forces can also be introduced by endowing the lattice's connecting ligaments with bending and torsional rigidity. We consider such a
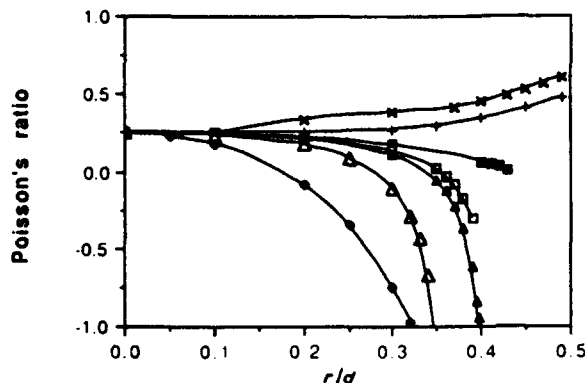
2289

*Figure 7* Chiral (noncentrosymmetric) hexagonal microstructure of rotatable nodes and bendable ligaments. Poisson's ratio is negative.

*Figure 6* Poisson's ratio versus rotatable node size, $r$, divided by lattice spacing, $d$, for non-central force lattice shown in Fig. 4, with prestrain in the ligaments. Prestrain factor, $f$, is the ratio of natural length of the vertical and horizontal ligaments to their length in the lattice, the lattice spacing. $k_3/k_1$ is a ratio of ligament stiffnesses. ($\blacksquare$) $k_3/k_1 = 1, f = 1$; ($\square$) $k_3/k_1 = 1/2, f = 1/2$; ($\blacktriangle$) $k_3/k_1 = 1/4, f = 1/2$; ($\triangle$) $k_3/k_1 = 1/8, f = 1/8$; ($\diamond$) $k_3/k_1 = 8, f = 8$; ($+$) $k_3/k_1 = 1/2, f = 2$; ($\times$) $k_3/k_1 = 1/4, f = 2$.

three-dimensional cubic lattice of points linked by extendable, bendable and twistable ribs [29]. Given arbitrary rib stiffnesses, the structure is orthotropic; however, we derive conditions on the ligament stiffnesses to achieve isotropy. We find the Poisson's ratio to be 1/4 for zero rib-bend stiffness. The bend rigidity of straight ribs reduces the Poisson's ratio by a small amount even if the ribs are thick. The lower bound on Poisson's ratio for this lattice is zero, and it is approached if the bend stiffness of the ribs can be made larger than the extensional stiffness.

For the structure in Fig. 4, let us introduce a prestrain in the vertical and horizontal ligaments, $k_1$. The corresponding prestrain is then determined for the ligaments. $k_3$, based on equilibrium considerations. Ligament stiffness is again kept positive. Poisson's ratio can be made either greater or less than 1/4 or can be made negative as shown in Fig. 6. End points on the curves in Figs 5 and 6 represent the allowable range for positive stiffness of all ligaments under the restriction of elastic isotropy. The model can also yield Poisson's ratios less than $-1$; the lattice is then unstable to small perturbations. Observe that the negative Poisson's ratios can be obtained only if both non-central forces and prestrain are present simultaneously.

### 2.4. Noncentrosymmetry

An unusual type of anisotropy is displayed by the hexagonal structure given in Fig. 7. The structure has a negative Poisson's ratio as can be appreciated by visualization or by making a model. The structure is not equivalent to its mirror image, so it lacks a centre of symmetry. Such structures are known as non-centrosymmetric, hemitropic, or chiral: they can be isotropic with respect to direction but by definition are not isotropic with respect to handedness. In contrast to the centrosymmetric lattice in Fig. 6, no prestrain is needed. The centres of the rigid nodes move in
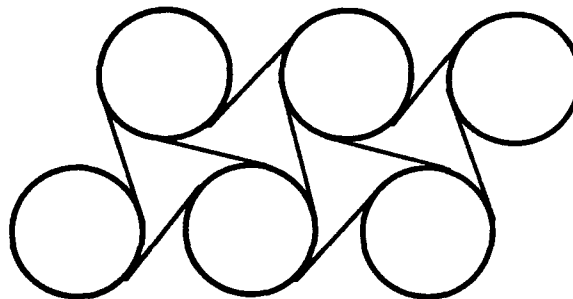
an affine manner. However, if we represent the structure as an assemblage of point particles, the "points" in the rigid nodes become connected by very stiff ligaments; in such a view the deformation becomes non-affine. A related "molecular" model was developed [30] which incorporated rotational degrees of freedom and a nearest neighbour inverse $n$th power interaction. Negative Poisson's ratios arose in this model if the molecules were given a preferred orientation or tilt. This is also a chiral structure, so despite the title given to reference [30] the structure is not isotropic. The tilting disc model in [11, 19] also appears to have a chiral asymmetry; however, it was not discussed by the authors.

## 3. Role of generalized continuum mechanics

The non-affine, rotational and noncentrosymmetric degrees of freedom considered above in a structural sense can also be viewed in the context of continuum mechanics. Continuum theories for elastic materials are available with different amounts of freedom: the uniconstant and classical elasticity theories discussed above are the simplest examples. Although the continuum and structural views are distinct, we consider insight gained in one perspective to be transferable to the other.

Cosserat elasticity [31], also known as micropolar elasticity [32], allows the points in the solid rotational freedom as well as translational freedom. Correspondingly there is a couple per unit area or couple stress as well as the usual stress which is a force per unit area. An isotropic Cosserat solid is described by six elastic constants. Conceptually, this continuum representation corresponds to a microstructure containing rotatable elements which support bending or torsional loads [29] or are connected by ligaments which can support such loads. It had been suggested that Cosserat elasticity could be a mechanism for negative Poisson's ratios [33], however the range for Poisson's ratio in a Cosserat solid is the same as that for classical elasticity [32, 34]. Cosserat solids differ from classical ones in that stress concentration factors differ from classical predictions, as does the rigidity of bars in bending and torsion. Such effects depend on the characteristic lengths which are additional elastic constants in Cosserat theory: if these lengths vanish,

2290

classical elasticity is obtained as a special case. If the strains in the object vary over scales comparable to the characteristic lengths, then the stress will differ significantly from classical predictions. Experiments have disclosed several materials to behave as Cosserat solids, but the Poisson's ratios are not unusual (see, e.g. [35]).

Chiral or noncentrosymmetric solids are those which are not invariant to an inversion of the coordinates. No mechanical effect of such asymmetry is predicted by classical elasticity. Cosserat elasticity allows the effects of chirality to be incorporated in a natural way; new effects are predicted such as the untwisting of a bar under tensile force, and size effects in Poisson's ratio [36].

Another generalized continuum theory is of elastic materials with microstructure [37], or micromorphic solids [38]. This theory allows the points in the solid to translate, rotate, and deform; the theory is therefore more general than classical elasticity or Cosserat elasticity, and an isotropic solid is described by 18 elastic constants. The allowable range for Poisson's ratio is nevertheless identical to that for classical elastic solids [39]. Because the local micro-deformation can differ from the macro-deformation, a micro-elastic solid of this type would experience non-affine deformation in the structural view.

Each structural mechanism considered here which gives rise to a negative Poisson's ratio is associated with a generalized continuum. Yet the generalized continuum theories allow the same range of Poisson's ratio as does classical elasticity. Not all solids which behave as generalized continua will have a negative Poisson's ratio; however, all negative Poisson's ratio materials will be describable as generalized continua. The characteristic lengths may be sufficiently small that the resulting nonclassical effects are too small to observe. Nevertheless the Poisson's ratio is a macroscopic result of the microstructure; it is measurable no matter how small the structure is. For materials in which the structure size is sufficiently large, nonclassical effects describable by generalized continuum mechanics can be substantial. It is important to consider which theory actually describes the material; for example Cosserat elasticity predicts a reduction of stress concentration factors for holes and cracks in comparison with classical values, while a different special case of microstructure elasticity predicts an increase [39, 40].

## 4. Discussion

Several structural mechanisms have been found to give rise to a negative Poisson's ratio: non-affine deformation, non-central force interaction combined with prestrain, and chiral structure combined with either non-central force or non-affine deformation. The materials originally reported [1] by the author have freedom to undergo both non-affine deformation and bending of the ligaments (hence noncentral force). Other materials which have been reported to have a negative Poisson's ratio are mostly anisotropic and exhibit the effect only in some directions; the mechanism of directional anisotropy has not been treated here. Rocks can be anisotropic; however, it is possible that the effects reported in rocks with microcracks [8, 9] are due to non-affine deformation in the opening of the microcracks. Theoretical analyses of the effect of microcracks [41] predict that when there are enough cracks to reduce the Poisson's ratio to zero, Young's modulus also becomes zero, so that negative Poisson's ratios are not predicted by these theories, and theory and experiment fail to agree in this case. Rocks can exhibit complex behaviour: the Poisson's ratio of rock can depend very much on the stress history [42]. Polymer gels represent another interesting class of materials: such gels can exhibit negative Poisson's ratios over a narrow temperature range during phase transitions [43]. The mechanism for this has not been elucidated; however, we surmise that prestrain is involved. It remains to be determined by experiment which structural mechanisms are most important in generating the effects in real materials such as the above.

Structural mechanisms are of interest in connection with the other material properties of materials with negative Poisson's ratios. For example, the non-affine mechanism is associated with an unfolding of the unit cells. Such unfolding results in a change in the relation between stress and strain under large deformation: the stress–strain curves for re-entrant foam tend to be more linear than those of conventional foams. As for dynamical aspects, the convoluted unit cells can vibrate and give rise to unusual acoustic behaviour [6] not explicitly associated with the Poisson's ratio. Moreover, it is possible that non-affine deformation kinematics can be exploited to make new materials with unusual and useful acoustic behaviour. As for density, the materials originally reported [1] were polymer foams of relatively low relative density (solid volume fraction) with cells of size 0.3–2.5 mm. The foam cells could, in principle, be arbitrarily small, down to molecular scale. The upper bound on the relative density of this type of material is not yet known; however, we have no doubt there is such a bound and that it is significantly less than unity. As for stiffness and strength, low density in cellular solids is associated with low stiffness, and although metal foam is much stiffer than polymer foam [1, 2], materials with negative Poisson's ratios with higher density would be of interest [44]. The possibility of making high-density "solids" based on non-central forces with prestrain, or on chiral structures, is an intriguing one. As for toughness and damage resistance, the Poisson's ratio itself has bearing upon the stress concentration factors in certain three-dimensional crack geometries [1] such that negative values of large magnitude are advantageous. The generalized continuum aspects of these materials also affect stress concentration factors. Consequently, the toughness and damage resistance of these materials is expected to depend on the deformation mechanisms described above and upon the cell size. Experiments are required to elucidate the connection.

Structural mechanisms are also of interest in connection with the fabrication of materials with

negative Poisson's ratios. It is now known that materials can be made which undergo non-affine deformation and rib bending [1, 2]. We have also made honeycombs based on the structures shown in Figs 2 and 7. However, many of the models which have been reported for materials with negative Poisson's ratios tend not to lend themselves to the making of materials. As for the present non-central force model with prestrain, it is possible that such prestrain could be introduced by selective crystallization and cooling. It remains to be seen whether materials with negative Poisson's ratios can be made in a controlled way based on the alternative models.

## 5. Conclusions

1. Negative Poisson's ratios can be obtained by a non-affine deformation geometry alone.

2. Negative Poisson's ratios can result from a combination of non-central forces and prestrain.

3. Negative Poisson's ratios can result from a chiral structure with rotational degrees of freedom combined with non-central force or non-affine deformation.

## References
1. R. S. LAKES, Science 235 (1987) 1038.
2. E. A. FRIIS, R. S. LAKES and J. B. PARK, J. Mater. Sci. 23 (1988) 4406.
3. R. S. LAKES, in "Developments in Mechanics", Vol. 14, Proceedings, 20th Midwest Mechanics Conference, Purdue University, 31 August–2 September 1987, pp. 758–63.
4. A. W. LIPSETT and A. I. BELTZER, J. Acoust. Soc. Amer. 84 (1988) 2179.
5. A. FREEDMAN, J. Sound Vibration 137 (1990) 209.
6. C. P. CHEN and R. S. LAKES, J. Cellular Polym. 8 (1989) 343.
7. L. J. GIBSON, M. F. ASHBY, G. S. SCHAJER and C. I. ROBERTSON, Proc. Roy. Soc. Lond. A382 (1982) 25.
8. F. HOMAND-ETIENNE and R. HOUPERT, Int. J. Rock Mech. Min. Sci. Geomech. Abstr. 26 (1989) 125.
9. A. NUR and G. SIMMONS, Earth Planet. Sci. Lett. 7 (1969) 183.
10. B. D. CADDOCK and K. E. EVANS, J. Phys. D Appl. Phys. 22 (1989) 1877.
11. K. E. EVANS and B. D. CADDOCK, ibid. 22 (1989) 1883.
12. C. T. HERAKOVICH, J. Compos. Mater. 18 (1985) 447.
13. S. W. TSAI and H. T. HAHN, "Introduction to composite materials" (Technomic, Lancaster, PA, 1980).
14. M. MIKI and Y. MOROTSU, JSME Int. J. 32 (1989) 67.
15. A. M. GARBER, Aerospace Engng 22 (1963) 126.
16. N. BETTENBOUCHE, G. A. SAUNDERS, E. F. LAMBSON and W. HÖNLE, J. Phys. D. Appl. Phys. 22 (1989) 670.
17. M. Ya. POPEREKA and V. G. BALAGUROV, Sov. Phys. Solid State 11 (1970) 2938.
18. R. F. ALMGREN, J. Elasticity 15 (1985) 427.
19. K. E. EVANS, J. Phys. D Appl. Phys. 22 (1989) 1870.
20. G. SIMMONS and H. WANG, "Single crystal elastic constants and calculated aggregate properties: a handbook", 2nd Edn (MIT Press, Cambridge, 1971).
21. J. H. WEINER, "Statistical Mechanics of Elasticity" (Wiley, NY, 1983).
22. S. P. TIMOSHENKO, "History of Strength of Materials" (Dover, NY, 1983).
23. A. E. H. LOVE, "A Treatise on the Mathematical Theory of Elasticity", 4th Edn (Dover, NY, 1944).
24. J. F. NYE, "Physical Properties of Crystals" (Clarendon Press, Oxford, 1976).
25. L. J. GIBSON and M. ASHBY, "Mechanics of cellular solids" (Pergamon, Oxford, New York, 1988).
26. A. G. KOLPAKOV, Prikl. Mat. Mekh. 59 (1985) 969.
27. K. BERGLUND, Arch. Mech. 29 (1977) 383.
28. R. J. BATHURST and L. ROTHENBURG, Int. J. Engng Sci. 26 (1988) 373.
29. T. R. TAUCHERT, Recent Adv. Engng Sci. 5 (1970) 325.
30. K. W. WOJCIECHOWSKI, Phys. Lett. A 137 (1989) 60.
31. E. and F. COSSERAT, "Théorie des Corps Déformables" (Hermann, Paris, 1909).
32. A. C. ERINGEN, in "Fracture", Vol. 1 (Academic, New York, 1968) pp. 621–729.
33. S. BURNS, Science 238 (1987) 551.
34. R. S. LAKES, ibid. 238 (1987) 551.
35. R. S. LAKES, Int. J. Solids Structures 22 (1986) 55.
36. R. S. LAKES and R. L. BENEDICT, Int. J. Engng Sci. 29 (1982) 1161.
37. R. D. MINDLIN, Arch. Rational Mech. Anal. 16 (1964) 51.
38. A. C. ERINGEN, "Mechanics of micromorphic continua", IUTAM symposium, "Mechanics of Generalized Continua", edited by E. Kröner (Springer Verlag, 1968).
39. J. L. BLEUSTEIN, Int. J. Solids Structures 2 (1960) 83.
40. S. C. COWIN, Q. J. Mech. Appl. Math. 37 (1984) 441.
41. E. D. CASE, J. Mater. Sci. 19 (1984) 3702.
42. O. G. INGLES, I. K. LEE and R. C. NEIL, Rock Mech. 5 (1973) 203.
43. S. HIROTSU, Macromol. 23 (1990) 903.
44. J. CHERFAS, Science 247 (1990) 630.